mixture of $CHCl_3$ (40 mL) and pyridine (0.32 mL, 3.97 mmol). Three portions of PBr_3 (3 × 0.05 mL, 1.58 mmol) were added dropwise every 30 min to the refluxing solution. After the last portion of PBr_3 was added, the reaction was refluxed for 2 h. The solution was cooled to room temperature, 2-propanol (20 mL) was added, and the reaction was stirred for an additional 10 min. The solution was washed with 1 N $NaHCO_3$ (3 × 50 mL) and dried ($MgSO_4$), and the solvent was removed in vacuo to give a white solid. The crude product was purified by flash column chromatography eluting with hexane/ethyl acetate (8:1) to give a slightly yellow solid (1.20 g, 53%). ^1H NMR (300 MHz, $CDCl_3$): δ 4.51 (s, 2H). ^{19}F NMR (282, MHz, $CDCl_3$): δ −150.50 (m, 2F), −141.80 (m, 2F).

Synthesis of 16−21. General Synthetic Procedure. GB (**2**) or GC (**3**) (0.07 mmol) was dissolved in THF (4 mL), and KH (0.008 g, 0.24 mmol) was added at room temperature. The reaction mixture was stirred for 10 min, and then, a solution of 4-(bromomethyl)benzophenone, **12**, or **15** (0.212 mmol) in THF (1 mL) was added dropwise. The reaction was stirred at room temperature for 4 h. The solution was then cooled to 0 °C, and concentrated HCl (0.3 mL) was added. The mixture was diluted with H_2O (10 mL), extracted with EtOAc (3 × 10 mL), and washed with saturated aqueous NH_4Cl solution (30 mL), brine (30 mL), and H_2O (30 mL). The organic phase was dried ($MgSO_4$), and the solvent was removed in vacuo. The crude material was purified by flash column chromatography using either A: $CHCl_3$/MeOH (100:1 and 50:1), B: $CHCl_3$/MeOH (30:1 and 20:1), or C: cyclohexane/acetone (3:1 and 2:1). All ginkgolide derivatives were white solids that decomposed above 250 °C.

10-*O*-Benzophenone Ginkgolide B (16). Purified by method B; yield, 0.035 g (78%). ^1H NMR (400 MHz, CD_3OD): δ 1.13 (s, *tert*-butyl), 1.24 (d, J = 7.1, CH_3), 1.92 (dd, J = 14.3, 4.5, 8-H), 2.07 (td, J = 13.9, 4.4, 7α-H), 2.27 (dd, J = 13.5, 4.6, 7β-H), 3.06 (q, J = 7.1, 14-H), 4.31 (d, J = 7.2, 1-H), 4.55 (d, J = 7.2, 2-H), 4.85 (d, J = 11.5, benzylic-H, 1H), 5.28 (s, 10-H), 5.42 (d, J = 4.0, 6-H), 5.59 (d, J = 11.5, benzylic-H, 1H), 6.15 (s, 12-H), 7.53−7.60 (m, Ar−H, 4H), 7.65−7.67 (m, Ar−H, 1H), 7.77−7.82 (m, Ar−H, 4H). ^{13}C NMR (100 MHz, CD_3OD): δ 7.25, 28.46 (3C), 32.18, 37.26, 42.29, 49.61, 68.21, 72.59, 72.80, 74.45, 76.76, 79.48, 83.53, 93.15, 99.78, 110.83, 127.96 (2C), 128.58 (2C), 130.03 (2C), 130.52 (2C), 132.94, 137.76 (2C), 141.67, 171.52, 172.70, 177.33, 196.45. HPLC−UV: 98.5%. HRMS: $C_{34}H_{34}O_{11}$ requires M + Na at *m/z* 641.1999; found, 641.2018.

10-*O*-Benzophenone Ginkgolide C (17). Purified by method A; yield, 0.023 g (64%). ^1H NMR (400, MHz, CD_3OD): δ 1.20 (s, *tert*-butyl), 1.24 (d, J = 7.1, CH_3,), 1.78 (d, J = 12.5, 8-H), 3.04 (q, J = 7.1, 14-H), 4.21 (dd, J = 12.5, 4.3, 7-H), 4.28 (d, J = 7.0, 1-H), 4.54 (d, J = 7.0, 2-H), 4.87 (d, J = 11.6, benzylic-H, 1H), 5.13 (d, J = 4.3, 6-H), 5.28 (s, 10-H), 5.60 (d, J = 11.6, benzylic-H, 1H), 6.17 (s, 12-H) 7.53−7.61 (m, Ar−H, 4H), 7.65−7.67 (m, Ar−H, 1H), 7.77−7.83 (m, Ar−H, 4H). ^{13}C NMR (100 MHz, CD_3OD): δ 7.34, 28.50 (3C), 32.12, 42.26, 50.00, 64.48, 67.40, 72.77, 74.28, 75.14, 76.74, 79.49, 83.55, 93.28, 99.54, 110.63, 127.95 (2C), 128.59 (2C), 130.03 (2C), 130.53 (2C), 132.96, 137.68 (2C), 141.65, 171.41, 172.55, 177.27, 197.03. HPLC−UV: 99.3%. HRMS: $C_{34}H_{34}O_{12}$ requires M + 1 at *m/z* 635.2129; found, 635.2098.

10-*O*-(Trifluoromethyl-3*H*-diazirine)benzyl Ginkgolide B (18). Purified by method B; yield, 0.024 g (59%). ^1H NMR (400 MHz, CD_3OD): δ 1.11 (s, *tert*-butyl), 1.23 (d, J = 7.1, CH_3), 1.89 (dd, J = 14.3, 4.3, 8-H), 2.01 (td, J = 13.9, 4.3, 7α-H), 2.25 (dd, J = 13.4, 4.4, 7β-H), 3.05 (q, J = 7.1, 14-H), 4.27 (d, J = 7.3, 1-H), 4.53 (d, J = 7.3, 2-H), 4.77 (d, J = 11.2, benzylic-H, 1H), 5.24 (s, 10-H), 5.39 (d, J = 3.9, 6-H), 5.51 (d, J = 11.2, benzylic-H, 1H), 6.14 (s, 12-H), 7.29 and 7.53 (AA'BB' system, Ar−H, 4H). ^{13}C NMR (75 MHz, $CDCl_3$): δ 7.67, 21.57 (q, $^2J_{CF}$ = 40.9, CCF_3), 29.56 (3C), 32.65, 37.49, 49.31, 68.07, 72.88, 73.57, 74.57, 76.56, 77.65, 80.08, 83.90, 90.90, 99.05, 110.68, 122.33 (q, $^1J_{CF}$ = 274.3, CF_3), 127.83 (2C), 129.53 (2C), 131.06, 136.44, 171.25, 171.50, 175.87. ^{19}F NMR (282 MHz, $CDCl_3$): δ −66.23 (s, 3F). HPLC−UV: 99.1%. HRMS: $C_{29}H_{29}F_3N_2O_{10}$ requires M + 1 at *m/z* 623.1853; found, 623.1834.

10-*O*-(Trifluoromethyl-3*H*-diazirine)benzyl Ginkgolide C (19). Purified by method A; yield, 0.023 g (51%). ^1H NMR (400 MHz, CD_3OD): δ 1.17 (s, *tert*-butyl), 1.24 (d, J = 7.1, CH_3,), 1.76 (d, J = 12.5, 8-H), 3.02 (q, J = 7.1, 14-H), 4.15 (dd, J = 12.5, 4.3, 7-H) 4.24 (d, J = 7.0, 1-H), 4.52 (d, J = 7.0, 2-H), 4.79 (d, J = 11.3, benzylic-H, 1H), 5.10 (d, J = 4.3, 6-H), 5.23 (s, 10-H), 5.52 (d, J = 11.3, benzylic-H, 1H), 6.15 (s, 12-H), 7.29 and 7.54 (AA'BB' system, aromatic-H, 4H). ^{13}C NMR (75 MHz, $CDCl_3$): δ 7.65, 23.77 (q, $^2J_{CF}$ = 38.9, CCF_3), 29.52 (3C), 32.65, 41.94, 50.92, 64.43, 67.48, 73.89, 74.30, 76.03, 76.34, 79.63, 83.90, 90.91, 98.94, 110.53, 122.32 (q, $^1J_{CF}$ = 275.0, CF_3), 127.94 (2C), 129.68 (2C), 131.26, 136.07, 170.97, 171.07, 175.69. ^{19}F NMR (282 MHz, $CDCl_3$): δ −66.25 (s, 3F). HPLC−UV: 97.9%. HRMS: $C_{29}H_{29}F_3N_2O_{11}$ requires M + 1 at *m/z* 639.1802; found, 639.1790.

10-*O*-Tetrafluorobenzyl Azide Ginkgolide B (20). Purified by method B; yield, 0.023 g (50%). ^1H NMR (400 MHz, $CDCl_3$): δ 1.13 (s, *tert*-butyl), 1.32 (d, J = 7.0, CH_3), 1.84−1.97 (m, 8-H and 7α-H), 2.27−2.33 (m, 7β-H), 2.84 (d, J = 3.5, 1-OH), 2.99 (s, 3-OH), 3.06 (q, J = 7.0, 14-H), 4.29 (dd, J = 7.9, 3.5, 1-H), 4.61 (d, J = 7.9, 2-H), 4.81 (d, J = 10.7, benzylic-H, 1H), 4.94 (s, 10-H), 5.39 (d, J = 3.4, 6-H), 5.64 (d, J = 10.7, benzylic-H, 1H), 6.03 (s, 12-H). ^{13}C NMR (100 MHz, $CDCl_3$): δ 7.70, 29.52 (3C), 32.62, 37.37, 42.03, 49.30, 61.21, 68.11, 72.79, 74.65, 80.07, 83.89, 91.00, 99.12, 108.95, 110.73, 139.71, 142.24, 144.45, 147.10, 170.69, 171.45, 175.83. ^{19}F NMR (282 MHz, $CDCl_3$): δ −143.31 (m, 2F), −150.85 (m, 2F). HPLC−UV: 98.8%. HRMS: $C_{27}H_{25}F_4N_3O_{10}$ requires M + 1 at *m/z* 628.1554; found, 628.1565.

10-*O*-Tetrafluorobenzyl Azide Ginkgolide C (21). Purified by method C; yield, 0.080 g (54%). ^1H NMR (400 MHz, $CDCl_3$): δ 1.22 (s, *tert*-butyl), 1.33 (d, J = 7.0, CH_3,), 1.71 (d, J = 12.4, 8-H), 2.33 (d, J = 10.6, 7-OH), 2.88 (d, J = 3.4, 1-OH), 3.01 (s, 3-OH), 3.08 (q, J = 7.0, 14-H), 4.08 (m, 7-H) 4.27 (dd, J = 7.8, 3.4, 1-H), 4.62 (d, J = 7.8, 2-H), 4.83 (d, J = 10.7, benzylic-H, 1H), 4.96 (s, 10-H), 5.09 (d, J = 4.4, 6-H), 5.58 (d, J = 10.7, benzylic-H, 1H), 6.04 (s, 12-H). ^{13}C NMR (75 MHz, $CDCl_3$): δ 7.64, 29.42 (3C), 32.59, 42.08, 50.64, 51.16, 61.47, 64.35, 67.32, 74.27, 75.88, 79.64, 83.88, 91.26, 99.14, 110.71, 120−150 (m, 6C), 170.72, 171.17, 176.29. ^{19}F NMR (282 MHz, $CDCl_3$): δ −143.56 (m, 2F), −151.08 (m, 2F). HPLC−UV: 99.1%. HRMS: $C_{27}H_{25}F_4N_3O_{11}$ requires M + 1 at *m/z* 644.1503; found, 644.1527.

10-*O*-Benzoylbenzoic Ginkgolide C (22). 4-Benzoylbenzoic acid (0.018 g, 0.08 mmol) and **2** (0.028 g, 0.07 mmol) were dissolved in THF (5 mL), and the mixture was cooled to 0 °C. EDC (0.018 g, 0.092 mmol) and DMAP (0.002 g, 0.01 mmol) were added, and the reaction mixture was stirred at 0 °C for 1 h and continued overnight at room temperature. The solvent was removed in vacuo, and the crude product was dissolved in EtOAc (20 mL) and washed with a saturated 5% $NaHCO_3$ solution (20 mL) and brine (20 mL). The organic fraction was dried ($MgSO_4$), and the solvent was evaporated in vacuo. The crude product was purified by flash column chromatography eluting with hexane/EtOAc (2:1) to give the product as white crystals (0.026 g, 62%). ^1H NMR (400 MHz, CD_3OD): δ 1.07 (s, *tert*-butyl), 1.26 (d, J = 7.1, CH_3), 1.98−2.10 (m, 8-H and 7α-H), 2.30−2.36 (m, 7β-H), 3.12 (q, J = 7.1, 14-H), 4.37 (d, J = 6.5, 1-H), 4.55 (d, J = 6.5, 2-H), 5.66 (d, J = 3.2, 6-H), 6.32 (s, 10-H), 6.45 (s, 12-H), 7.54−7.58 (m, Ar−H, 2H), 7.67−7.69 (m, Ar−H, 1H), 7.80−7.83 (m, Ar−H, 2H), 7.86−7.88 (m, Ar−H, 2H), 8.42−8.44 (m, Ar−H, 2H). ^{13}C NMR (100 MHz, CD_3OD): δ 7.42, 28.22 (3C), 32.16, 37.27, 42.29, 49.42, 67.81, 70.64, 72.74, 74.42, 79.29, 83.64, 95.13, 100.51, 111.12, 128.73 (2C), 129.92 (2C), 130.17 (2C), 130.58 (2C), 131.61, 133.41, 137.06, 142.66, 164.56, 168.93, 171.41, 177.33, 196.48. HPLC−UV: 99.2%. HRMS: $C_{34}H_{31}O_{12}$ requires M + Na at *m/z* 655.1791; found, 655.1790.

10-*O*-Benzophenone-7-*O*-dansyl Ginkgolide C (23). A solution of dansyl chloride (0.010 g, 0.035 mmol) in acetonitrile (0.3 mL) was added to a solution of **17** (0.020 g, 0.032 mmol) and DMAP (0.008 g, 0.063 mmol) in acetonitrile (1.5 mL). The reaction mixture was stirred for 16 h at room temperature, then a saturated aqueous NH_4Cl solution (2 mL) was added,

and the mixture was extracted with EtOAc (3 × 5 mL). The combined organic phase was washed with saturated aqueous NaCl solution (3 × 15 mL), dried ($MgSO_4$), and the solvent was removed in vacuo. The crude product was purified by flash column chromatography eluting with cyclohexane/acetone (2:1) to give the product as a slightly yellow solid (0.015 g, 56%). ^{1}H NMR (400 MHz, DMSO-d_6): δ 0.83 (s, *tert*-butyl), 1.09 (d, J = 7.2, CH_3,), 1.94 (d, J = 12.5, 8-H), 2.81 [m, 14-H and $N(CH_3)_2$], 4.26 (t, J = 5.3, 1-H), 4.53 (d, J = 5.4, 2-H), 4.79 (d, J = 13.2, benzylic-H, 1H), 4.89 (dd, J = 12.5, 4.0, 7-H), 5.19 (d, J = 4.0, 6-H), 5.23 (s, 10-H), 5.46 (d, J = 13.2, benzylic-H, 1H), 6.07 (d, J = 5.3, 1-OH), 6.21 (s, 12-H), 6.51 (s, 3-OH), 7.28–7.30 (m, Ar–H, 1H), 7.50–7.70 (m, Ar–H, 7H), 7.79–7.82 (m, Ar–H, 4H), 8.18–8.20 (m, Ar–H, 2H), 8.54–8.56 (m, Ar–H, 1H). HPLC–UV: 98.9%. HRMS: $C_{46}H_{45}NO_{14}S$ requires M + 1 at *m/z* 868.2639; found, 868.2642.

10-*O*-benzophenone-1-*O*-dansyl Ginkgolide C (24). Synthesized as **23** but using 2 equiv of dansyl chloride (instead of 1.1 equiv) gave rise to a ca. 1:1 mixture of **23** and **24**. The two products were separated on analytical TLC giving **24** (0.008 g, 30%) as a slightly yellow solid. ^{1}H NMR (400 MHz, DMSO-d_6): δ 0.91 (s, *tert*-butyl), 1.16 (d, J = 7.6, CH_3,), 1.78 (d, J = 12.5, 8-H), 2.80 [s, $N(CH_3)_2$], 2.97 (q, J = 7.6, 14-H), 4.22 (d, J = 3.8, 1-H), 4.26 (m, 7-H), 4.57 (d, J = 3.9, 6-H), 4.80 (d, J = 13.2, benzylic-H, 1H), 5.20 (d, J = 3.8, 2-H), 5.30 (s, 10-H), 5.31 (d, J = 4.9, 7-OH), 5.49 (d, J = 13.2, benzylic-H, 1H), 5.95 (s, 12-H), 5.98 (s, 3-OH), 7.25–7.27 (m, Ar–H, 1H), 7.54–7.79 (m, Ar–H, 11H), 8.18–8.24 (m, Ar–H, 2H), 8.47–8.49 (m, Ar–H, 1H). HPLC–UV: 99.0%. HRMS: $C_{46}H_{45}NO_{14}S$ requires M + 1 at *m/z* 868.2639; found, 868.2668.

Radioligand Binding Assay. Heart and skeletal muscles from 13 to 27 months old PAFR transgenic (PAFR-Tg) mice,[62] which overexpress guinea pig PAFR, were homogenized in a Polytron homogenizer in cold buffer A [25 mM Hepes/NaOH (pH 7.4), 0.25 M sucrose, 10 mM $MgCl_2$, 1 mM PMSF, and a protease inhibitor cocktail Complete (Boehringer Mannheim)]. An 800*g* (for 10 min) supernatant of the homogenate was centrifuged at 100 000*g* at 4 °C for 1 h, and the resulting pellet was suspended in buffer A and stored at −80 °C until use. The protein concentration of the suspended membrane fraction was 1.37 mg/mL, as measured by the method of Bradford[63] using the Bio-Rad protein assay solution and fatty acid-free bovine serum albumin (BSA; Bayer, Kankakee, IL) as a standard. The radioligand binding assays were performed essentially as previously described.[53] The membrane fractions from hearts and skeletal muscles of PAFR-Tg mice (50 μL of suspension containing 121 fmol of PAFR) were mixed with 2 pmol of [^{3}H]WEB 2086 (NEN Life Science Products, Boston, MA) in 50 μL of buffer B [25 mM Hepes/NaOH (pH 7.4), 0.25 M sucrose,10 mM $MgCl_2$, 0.1% BSA], and the compound was to be tested in 100 μL of buffer B in a 96 well microplate in triplicate for each concentration. These mixtures were incubated at 25 °C for 90 min, upon which the receptor-bound [^{3}H]-WEB 2086 was filtered on a UniFilter-GF/C (Packard Bioscience, Meriden, CT) using a MicroMate 196 simultaneous 96 well harvester (Packard Bioscience). The filter was then washed 10 times with cold buffer B and dried at 50 °C for at least 90 min, 25 μL of MicroScint-0 scintillation cocktail (Packard Bioscience) was added, and filters were placed in a TopCount microplate scintillation counter (Packard Bioscience). Binding data were analyzed with the nonlinear curve-fitting program Microplate Manager III (Bio-Rad, Hercules, CA). Calculated IC_{50} values were then converted to K_i values using the Cheng–Prusoff correction,[64] with the following equation: $K_i = IC_{50}/(1 + [L]/K_D)$, where [L] is the concentration of the radioligand, and K_D is the previously determined dissociation constant for [^{3}H]WEB 2086 (4.3 nM).[53] Nonspecific binding was determined using methods as previously described.[53]

Intracellular Calcium Mobilization. CHO cells expressing human PAFR[57] were subjected to the calcium assay as described previously[56] except that Fura-2/AM was loaded in the presence of chromophore EL (0.01%, Sigma). Each compound (100 μM) was applied to the cell suspension, and then, PAF (10 nM) was added after 3 min.

Acknowledgment. We are grateful to Dr. Yasuhiro Itagaki for performing HRMS. We thank the Alfred Benzon Foundation (to K.S.) and the NSF REU program (CHE 9820490, to D.R.S., Beloit College, Beloit, WI) for financial support.

References

(1) Drieu, K.; Jaggy, H. History, development and constituents of EGb 761. In *Medicinal and Aromatic Plants-Industrial Profiles: Ginkgo biloba*; van Beek, T. A., Ed.; Harwood Academic Publishers: Amsterdam, 2000; Vol. 12, pp 267–277.
(2) Hasler, A. Chemical constituents of Ginkgo biloba. In *Medicinal and Aromatic Plants-Industrial Profiles: Ginkgo biloba*; van Beek, T. A., Ed.; Harwood Academic Publishers: Amsterdam, 2000; Vol. 12, pp 109–142.
(3) Nakanishi, K. The ginkgolides. *Pure Appl. Chem.* **1967**, *14*, 89–113 and references therein.
(4) Okabe, K.; Yamada, K.; Yamamura, S.; Takada, S. Ginkgolides. *J. Chem. Soc. C* **1967**, 2201–2206.
(5) Nakanishi, K.; Habaguchi, K.; Nakadaira, Y.; Woods, M. C.; Maruyama, M.; Major, R. T.; Alauddin, M.; Patel, A. R.; Weinges, K.; Bähr, W. Structure of bilobalide, a rare *tert*-butyl containing seuqiterpenoid related to the C_{20}-ginkgolides. *J. Am. Chem. Soc.* **1971**, *93*, 3544–3546.
(6) Weinges, K.; Hepp, M.; Jaggy, H. Chemie der Ginkgolide, II. Isolierung und Strukturaufklärung eines neuen Ginkgolids *Liebigs Ann. Chem.* **1987**, 521–526.
(7) DeFeudis, F. V.; Drieu, K. Ginkgo biloba extract (EGb 761) and CNS functions: basic studies and clinical applications *Curr. Drug Targets* **2000**, *1*, 25–58.
(8) Logani, S.; Chen, M. C.; Tran, T.; Le, T.; Raffa, R. B. Actions of Ginkgo biloba related to potential utility for the treatment of conditions involving cerebral hypoxia. *Life Sci.* **2000**, *67*, 1389–1396.
(9) Oken, B. S.; Storzbach, D. M.; Kaye, J. A. The efficacy of Ginkgo biloba on cognitive function in alzheimer disease. *Arch. Neurol.* **1998**, *55*, 1409–1415.
(10) Kleijnen, J.; Knipschild, P. Ginkgo biloba. *Lancet* **1992**, *340*, 1136–1139.
(11) Søholm, B. Clinical improvement of memory and other cognitive functions by Ginkgo biloba: review of relevant literature. *Adv. Nat. Ther.* **1998**, *15*, 54–65.
(12) Diamond, B. J.; Shiflett, S. C.; Feiwel, N.; Mathies, R. J.; Noskin, O.; Richards, J. A.; Schoenberger, N. E. Ginkgo biloba extract: mechanisms and clinical indications. *Arch. Phys. Med. Rehabil.* **2000**, *81*, 668–678.
(13) van Dongen, M. C. J. M.; van Rossum, E.; Knipschild, P. Efficacy of Ginkgo biloba special extracts – evidence from randomized clinical trials. In *Medicinal and Aromatic Plants-Industrial Profiles: Ginkgo biloba*; van Beek, T. A., Ed.; Harwood Academic Publishers: Amsterdam, 2000; Vol. 12, pp 385–442.
(14) Le Bars, P. L.; Katz, M. M.; Berman, N.; Itil, T. M.; Freedman, A. M.; Schatzberg, A. F. A placebo-controlled double-blind, randomized trial of an extract of Ginkgo biloba for dementia. North American EGb study group. *J. Am. Med. Assoc.* **1997**, *278*, 1327–1332.
(15) Kanowski, S.; Hermann, W. M.; Stephan, K.; Wierich, W.; Horr, R. Proof of efficacy of Ginkgo biloba special extract EGb 761 in outpatients suffering from mild to moderate primary degenerative dementia of the Alzheimer type or multi-infarct dementia. *Pharmacopsychiatry* **1996**, *29*, 47–56.
(16) Watanabe, M. H.; Wolffram, S.; Ader, P.; Rimbach, G.; Packer, L.; Maguire, J. J.; Schultz, P. G.; Gohil, K. The in vivo neuromodulatory effects of the herbal medicine Ginkgo biloba. *Proc. Natl. Acad. Sci. U.S.A.* **2001**, *98*, 6577–6580.
(17) Kennedy, D. O.; Scholey, A. B.; Wesnes, K. A. The dose-dependent cognitive effects of acute administration of Ginkgo biloba to healthy young volunteers. *Psychopharmacology* **2000**, *151*, 416–423.
(18) Polich, J.; Gloria, R. Cognitive effects of a Ginkgo biloba/vinpocetine compound in normal adults: systematic assessment of perception, attention and memory. *Hum. Psychopharmacol. Clin. Exp.* **2001**, *16*, 409–416.
(19) Rigney, U.; Kimber, S.; Hindmarch, I. The effects of acute doses of standardized Ginkgo biloba extract on memory and psychomotor performances in volunteers. *Phytother. Res.* **1999**, *13*, 408–415.
(20) Stough, C.; Clarke, J.; Lloyd, J.; Nathan, P. J. Neuropsychological changes after 30-day Ginkgo biloba administration in healthy patients. *Int. J. Neuropsychopharmacol.* **2001**, *4*, 131–134.

(21) Braquet, P.; Spinnewyn, B.; Braquet, M.; Bourgain, R. H.; Taylor, J. E.; Etienne, A.; Drieu, K. BN 52021 and related compounds: a new series of highly specific PAF-acether antagonists isolated from Ginkgo biloba L. *Blood Vessels* **1985**, *16*, 559–572.
(22) Ishii, S.; Shimizu, T. Platelet-activating factor (PAF) receptor and genetically engineered PAF receptor mutant mice. *Prog. Lipid Res.* **2000**, *39*, 41–82.
(23) Prescott, S. M.; Zimmerman, G. A.; Stafforini, D. M.; McIntyre, T. M. Platelet-activating factor and related lipid mediators. *Annu. Rev. Biochem.* **2000**, *69*, 419–445.
(24) Shukla, S. D. Platelet activating factor. *Biomembranes* **1996**, *2B*, 463–479.
(25) Bito, H.; Nakamura, M.; Honda, Z.; Izumi, T.; Iwatsubo, T.; Seyama, Y.; Ogura, A.; Kudo, Y.; Shimizu, T. Platelet-activating factor (PAF) receptor in rat brain: PAF mobilizes intracelluar Ca^{2+} in hippocampal neurones. *Neuron* **1992**, *9*, 285–294.
(26) Mori, M.; Aihara, M.; Kume, K.; Hamanoue, M.; Kohsaka, S.; Shimizu, T. Predominant expression of platelet-activating factor receptor in the rat brain microglia. *J. Neurosci.* **1996**, *16*, 3590–3600.
(27) Kroegel, C.; Kortsik, C.; Kroegel, N.; Matthys, H. The pathophysiological role and therapeutic implications of platelet activating factor in diseases of aging. *Drugs Aging* **1992**, *2*, 345–355.
(28) Perry, S. W.; Hamilton, J. A.; Tjoelker, L. W.; Dbaibo, G.; Dzenko, K. A.; Epstein, L. G.; Hannun, Y.; Whittaker, J. S.; Dewhurst, S.; Gelbard, H. A. Platelet-activating factor receptor activation. An initiator step in HIV-1 neuropathogenesis. *J. Biol. Chem.* **1998**, *273*, 17660–17664.
(29) Kato, K.; Clark, G. D.; Bazan, N. G.; Zorumski, C. F. Platelet-activating factor as a potential retrograde messenger in CA1 hippocampal long-term potentiation. *Nature* **1994**, *367*, 175–179.
(30) Kornecki, E.; Wieraszko, A.; Chan, J. C.; Ehrlich, Y. H. Platelet activating factor (PAF) in memory formation: Role as a retrograde messenger in long-term potentiation. *J. Lipid Mediators Cell Signalling* **1996**, *14*, 115–126.
(31) Chen, C.; Magee, J. C.; Marcheselli, V.; Hardy, M.; Bazan, N. G. Attenuated LTP in hippocampal dentate gyrus neurons of mice deficient in the PAF receptor. *J. Neurophysiol.* **2001**, *85*, 384–390.
(32) Kobayashi, K.; Ishii, S.; Kume, K.; Takahashi, T.; Shimizu, T.; Manabe, T. Platelet-activating factor receptor is not required for long-term potentiation in the hippocampal CA1 region. *Eur. J. Neurosci.* **1999**, *11*, 1313–1316.
(33) Smith, P. F.; Maclennan, K.; Darlington, C. L. The neuroprotective properties of the Ginkgo biloba leaf: a review of the possible relationship to platelet-activating factor (PAF). *J. Ethnopharmacol.* **1996**, *50*, 131–139.
(34) Smith, P. F.; Maclennan, K. The therapeutic potential of PAF receptor antagonists in CNS disorders. *Curr. Opin. Anti-Inflammatory Immunomodulatory Invest. Drugs* **1999**, *1*, 205–218.
(35) Corey, E. J.; Ghosh, A. K. Total synthesis of ginkgolide A. *Tetrahedron Lett.* **1988**, *29*, 3205–3206.
(36) Corey, E. J.; Kang, M. C.; Desai, M. C.; Ghosh, A. K.; Houpis, I. N. Total synthesis of (±)-ginkgolide B. *J. Am. Chem. Soc.* **1988**, *110*, 649–651.
(37) Corey, E. J.; Su, W. G. Total synthesis of a C_{15} ginkgolide, (±)-bilobalide. *J. Am. Chem. Soc.* **1987**, *109*, 7534–7536.
(38) Corey, E. J.; Gavai, A. V. Simple analogues of ginkgolide B which are highly active antagonists of platelet activating factor. *Tetrahedron Lett.* **1989**, *30*, 6959–6962.
(39) Corey, E. J.; Rao, K. S. Enantioselective total synthesis of ginkgolide derivatives lacking the *tert*-butyl group, an essential structural subunit for antagonism of platelet activating factor. *Tetrahedron Lett.* **1991**, *32*, 4623–4626.
(40) Park, P.-U.; Pyo, S.; Lee, S.-K.; Sung, J. H.; Kwak, W. J.; Park, H.-K.; Cho, Y.-B.; Ryu, G. H.; Kim, T. S. Ginkgolide derivatives. U.S. Patent 5,541,183, 1996.
(41) Hu, L.; Chen, Z.; Cheng, X.; Xie, Y. Chemistry of ginkgolides: structure–activity relationship as PAF antagonists. *Pure Appl. Chem.* **1999**, *71*, 1153–1156.
(42) Hu, L.; Chen, Z.; Xie, Y.; Jiang, H.; Zhen, H. Alkyl and alkoxycarbonyl derivatives of ginkgolide B: synthesis and biological evaluation of PAF inhibitory activity. *Bioorg. Med. Chem.* **2000**, *8*, 1515–1521.
(43) Hu, L.; Chen, Z.; Xie, Y.; Jiang, Y.; Zhen, H. New products from alkali fusion of ginkgolides A and B. *J. Asian Nat. Prod. Res.* **2000**, *2*, 103–110.
(44) Hu, L.; Chen, Z.; Xie, Y. Synthesis and biological activity of amide derivatives of ginkgolide A. *J. Asian Nat. Prod. Res.* **2001**, *3*, 219–227.
(45) Dorman, G.; Prestwich, G. D. Using photolabile ligands in drug discovery and development. *Trends Biotechnol.* **2000**, *18*, 64–77.
(46) Flemming, S. A. Chemical reagents in photoaffinity labeling. *Tetrahedron* **1995**, *51*, 12479–12520.
(47) Kotzyba-Hilbert, F.; Kapfer, I.; Goeldner, M. Recent trends in photoaffinity labeling. *Angew. Chem., Int. Ed. Engl.* **1995**, *34*, 1296–1312.
(48) Nassal, M. 4-(1-Azi-2,2,2-trifluoroethyl)benzoic acid, a highly photolabile carbene generating label readily fixable to biochemical agents. *Liebigs Ann. Chem.* **1983**, 1510–1523.
(49) Nassal, M. 4′-(1-Azi-2,2,2-trifluoroethyl)phenylalanine, a photolabile carbene-generating analogue of phenylalanine. *J. Am. Chem. Soc.* **1984**, *106*, 7540–7545.
(50) Keana, J. F. W.; Cai, S. X. New reagents for photoaffinity labeling: synthesis and photolysis of functionalized perfluorophenyl azides. *J. Org. Chem.* **1990**, *55*, 3640–3647.
(51) Lei, H.; Marks, V.; Pasquale, T.; Atkinson, J. K. Synthesis of photoaffinity label analogues of α-tocopherol. *Bioorg. Med. Chem. Lett.* **1998**, *8*, 3453–3458.
(52) Lei, H.; Atkinson, J. Synthesis of phytyl- and chroman-derivatized photoaffinity labels based on α-tocopherol. *J. Org. Chem.* **2000**, *65*, 2560–2567.
(53) Shindou, H.; Ishii, S.; Uozumi, N.; Shimizu, T. Roles of cytosolic phopholipase A2 and platelet-activating factor receptor in the Ca-induced biosynthesis of PAF. *Biochem. Biophys. Res. Commun.* **2000**, *271*, 812–817.
(54) Li, H.; Liu, Y.; Fang, K.; Nakanishi, K. A simple photoaffinity labeling protocol. *Chem. Commun.* **1999**, 365–366.
(55) Maclennan, K. M.; Smith, P. F.; Darlington, C. L. The effects of ginkgolide B (BN52021) on guinea pig vestibular nucleus neurons in vitro: importance of controlling for effects of dimethyl sulfoxide (DMSO) vehicles. *Neurosci. Res.* **1996**, *26*, 395–399.
(56) Fukunaga, K.; Ishii, S.; Asano, K.; Yokomizo, T.; Shiomi, T.; Shimizu, T.; Yamaguchi, K. Single nucleotide polymorphism of human platelet-activating factor receptor impairs G-protein activation. *J. Biol. Chem.* **2001**, *276*, 43025–43030.
(57) Aoki, Y.; Nakamura, M.; Kodama, H.; Matsumoto, T.; Shimizu, T.; Noma, M. A radioreceptor binding assay for platelet-activating factor (PAF) using membranes from CHO cells expressing human PAF receptor. *J. Immunol. Methods* **1995**, *186*, 225–231.
(58) Corey, E. J.; Rao, K. S.; Ghosh, A. K. Intramolecular and intermolecular hydroxyl reactivity differences in ginkgolides A, B and C and their chemical applications. *Tetrahedron Lett.* **1992**, *33*, 6955–6958.
(59) Weinges, K.; Schick, H. Chemie der Ginkgolid IV. Herstellung von Ginkgolid B aus Ginkgolid C. *Liebigs Ann. Chem.* **1991**, 81–83.
(60) Chen, J.; Hu, L.; Jiang, H.; Gu, J.; Zhu, W.; Chen, Z.; Chen., K.; Ji, R. A 3D-QSAR study on ginkgolides and their analogues with comparative molecular field analysis. *Bioorg. Med. Chem. Lett.* **1998**, *8*, 1291–1296.
(61) van Beek, T. A.; Lelyved, G. P. Preparative isolation and separation procedure for ginkgolides A, B, C, and J and bilobalide. *J. Nat. Prod.* **1997**, *60*, 735–738.
(62) Ishii, S.; Nagase, T.; Tashiro, F.; Ikuta, K.; Sato, S.; Waga, I.; Kume, K.; Miyazaki, J.; Shimizu, T. Bronchial hyperreactivity, increased endotoxin lethality and melanocytic tumorigenesis in transgenic mice overexpressing platelet-activating factor receptor. *EMBO J.* **1997**, *16*, 133–142.
(63) Bradford, M. M. A rapid and sensitive method for the quantitation of microgram quantities of protein utilizing the principle of protein-dye binding. *Anal. Biochem.* **1976**, *72*, 248–254.
(64) Cheng, Y.; Prusoff, W. H. Relationship between the inhibition constant (K_i) and the concentration of inhibitor which causes 50% inhibition (I_{50}) of an enzymatic reaction. *Biochem. Pharmacol.* **1973**, *22*, 3099–3103.

JM020147W

Am J Physiol Heart Circ Physiol 282: H2024–H2030, 2002.
First published January 31, 2002; 10.1152/ajpheart.00956.2001.

Block of the background K^+ channel TASK-1 contributes to arrhythmogenic effects of platelet-activating factor

ANDREA BARBUTI,[1] SATOSHI ISHII,[2] TAKAO SHIMIZU,[2]
RICHARD B. ROBINSON,[1] AND STEVEN J. FEINMARK[1]
[1]*Center for Molecular Therapeutics, Department of Pharmacology, Columbia University, New York, New York 10032; and* [2]*Department of Biochemistry and Molecular Biology, University of Tokyo, Tokyo, 113-003 Japan*

Received 2 November 2001; accepted in final form 30 January 2002

Barbuti, Andrea, Satoshi Ishii, Takao Shimizu, Richard B. Robinson, and Steven J. Feinmark. Block of the background K^+ channel TASK-1 contributes to arrhythmogenic effects of platelet-activating factor. *Am J Physiol Heart Circ Physiol* 282: H2024–H2030, 2002. First published January 31, 2002; 10.1152/ajpheart.00956.2001.—Platelet-activating factor (PAF), an inflammatory phospholipid, induces ventricular arrhythmia via an unknown ionic mechanism. We can now link PAF-mediated cardiac electrophysiological effects to inhibition of a two-pore domain K^+ channel [TWIK-related acid-sensitive K^+ background channel (TASK-1)]. Superfusion of carbamyl-PAF (C-PAF), a stable analog of PAF, over murine ventricular myocytes causes abnormal automaticity, plateau phase arrest of the action potential, and early afterdepolarizations in paced and quiescent cells from wild-type but not PAF receptor knockout mice. C-PAF-dependent currents are insensitive to Cs^+ and are outwardly rectifying with biophysical properties consistent with a K^+-selective channel. The current is blocked by TASK-1 inhibitors, including protons, Ba^{2+}, Zn^{2+}, and methanandamide, a stable analog of the endogenous lipid ligand of cannabanoid receptors. In addition, when TASK-1 is expressed in CHO cells that express an endogenous PAF receptor, superfusion of C-PAF decreases the expressed current. Like C-PAF, methanandamide evoked spontaneous activity in quiescent myocytes. C-PAF- and methanandamide-sensitive currents are blocked by a specific protein kinase C (PKC) inhibitor, implying overlapping signaling pathways. In conclusion, C-PAF blocks TASK-1 or a closely related channel, the effect is PKC dependent, and the inhibition alters the electrical activity of myocytes in ways that would be arrhythmogenic in the intact heart.

two-pore domain potassium channels; Kcnk3 ventricular myocytes; inflammatory lipids; mouse

LETHAL ARRHYTHMIAS commonly occur after myocardial ischemia, especially when the ischemic myocardium is reperfused. These arrhythmias are usually initiated by ectopic activity triggered by early (EADs) and delayed afterdepolarizations (DADs) of the membrane potential. One consequence of ischemia and reperfusion is a rapid migration of polymorphonuclear leukocytes (PMNL) into the infarcted zone. Activated PMNL bind to activated myocytes and release several substances, including oxygen radicals, proteolytic enzymes, and inflammatory lipids that increase the extent of myocardial injury (15). Depletion of circulating neutrophils or treatment with anti-inflammatory drugs effectively limits the size of the infarct zone and the extent of the damage in hearts from several species (15, 20, 22)

Hoffman et al. (4, 5) demonstrated that activation of PMNL bound to isolated canine myocytes dramatically changed the myocyte transmembrane action potential. These changes included prolongation of the action potential duration (APD), EADs, and in some cases arrest during the plateau phase of the action potential. It was also shown that direct superfusion of myocytes with the inflammatory phospholipid platelet-activating factor (PAF) mimicked the action of activated PMNL and that, under similar conditions, PMNL produce significant levels of PAF. Furthermore, incubation of myocytes with the PAF receptor (PAFR) antagonist CV-6209 prevented both PAF- and PMNL-induced changes in myocyte membrane potential. PAF also induces arrhythmias in mice that overexpress the PAFR when the lipid is administered at intravenous doses that have little effect on wild-type (WT) animals (7). These observations suggested that PMNL-derived PAF could induce triggered activity and thus ventricular arrhythmias.

There is considerable confusion regarding the molecular mechanisms by which PAF could alter the electrical activity of the heart. Although PAF binds to a cell surface, G protein-linked receptor and ultimately increases cytosolic Ca^{2+} levels (17, 19), little is known about the effects of PAF on membrane channels. Wahler et al. (26) showed that subnanomolar concentrations of PAF markedly decreased the inwardly rectifying K^+ channel (I_{K1}) in guinea pig ventricular myocytes, whereas Hoffman et al. (5) suggested that depolarizing Na^+ current may play a role in the arrhythmogenic action of PAF.

Address for reprint requests and other correspondence: S. J. Feinmark, Center for Molecular Therapeutics, Dept. of Pharmacology, Columbia Univ., 630 W168th St., New York, NY 10032 (E-mail: sjf1@columbia.edu).

The costs of publication of this article were defrayed in part by the payment of page charges. The article must therefore be hereby marked "*advertisement*" in accordance with 18 U.S.C. Section 1734 solely to indicate this fact.

0363-6135/02 $5.00 Copyright © 2002 the American Physiological Society

Taking advantage of genetically modified mice in which PAFR have been knocked out [knockout (KO) mice] (6), we tested the ability of carbamyl-PAF (C-PAF), a nonmetabolizable PAF analog, to alter the membrane potential of isolated murine ventricular myocytes with the intent of clarifying the mechanisms determining the arrhythmogenic effects of this lipid.

METHODS

Cell preparation. Adult mice, 2–3 mo old, were anesthetized with ketamine-xylazine, and their hearts were removed according to protocols approved by the Columbia University Institutional Animal Care and Use Committee. Experiments were performed on single, rod-shaped, quiescent ventricular myocytes dissociated using a standard retrograde collagenase perfusion (11) from hearts of mice that were either WT or PAFR KO. Both WT and KO mice were bred on a C57/Bl6 background. The derivation of the KO mice has been described previously (5).

Heterologous expression. The TWIK-related acid-sensitive K^+ background channel (TASK-1) clone (provided by Professor Y. Kurachi, Osaka University; Osaka, Japan) was cotransfected in CHO cells with CD8 plasmid using Lipofectamine Plus (Invitrogen) according to the manufacturer's instructions. Forty-eight hours later, cells were transferred to the electrophysiology chamber, and anti-CD8-coated beads (Dynal Biotech) were added to identify CD8-expressing cells. The CD8-expressing cells were voltage clamped using a ramp clamp (see *Electrophysiological recordings*). CHO cells were used in these experiments in part because they express endogenous PAFR.

Buffers and drugs. Before electrophysiological measurements, cells were placed into the perfusion chamber and superfused at room temperature with Tyrode buffer [containing (in mM) 140 NaCl, 5.4 KCl, 1 $CaCl_2$, 1 $MgCl_2$, 5 HEPES, and 10 glucose; pH 7.4]. The whole cell patch-clamp technique was used with pipettes having resistances of 1.5–3 MΩ [the intracellular solution contained (in mM) 130 aspartic acid, 146 KOH, 10 NaCl, 2 $CaCl_2$, 5 EGTA, 10 HEPES, and 2 MgATP; pH 7.2]. Solutions of C-PAF, the PAFR antagonist CV-6209 (BIOMOL), and the protein kinase C (PKC) inhibitor bisindolylmaleimide I (BIM I; Calbiochem) were prepared in water and diluted in Tyrode buffer before use. An inactive analog of BIM I (BIM V; Calbiochem), anandamide, its nonhydrolyzable analog, methanandamide, and an inhibitor of anandamide hydrolysis, arachidonyltrifluoromethyl ketone (ATFK) (BIOMOL), were dissolved in DMSO and then diluted in Tyrode buffer. The final DMSO concentration did not exceed 0.1%. A custom-made fast perfusion device was used to exchange the solution around the cell within 1 s (2).

Electrophysiological recordings. Current and voltage protocols were generated using Clampex 7.0 software applied by means of an Axopatch 200B amplifier and a Digidata 1200 interface (Axon Instruments). During voltage clamp, steady-state current traces were acquired at 500 Hz and final filtered at 10 Hz. During current clamp, membrane voltage was acquired at 5 kHz and filtered at 1 kHz. Ramp clamps were conducted by imposing a voltage ramp (14 mV/s) at an acquisition rate of 500 Hz with 1-kHz filtering. Data were analyzed using pCLAMP 8.0 (Axon) and Origin 6.0 (Microcal) and are presented as means ± SE. Steady-state current was determined by computer calculation of average current over a time period of at least 5 s. In all experiments, the n value indicates the number of myocytes studied and represents pooled data from at least two (voltage clamp) or three (current clamp) animals. Student's t-test, one-way ANOVA, and χ^2-tests were used; a value of $P < 0.05$ was considered statistically significant. Records have been corrected for the junction potential, which was measured to be 9.8 mV.

RESULTS

C-PAF alters the rhythm of paced, WT ventricular myocytes. Myocytes from WT mice were paced (cycle length, 1,000 ms) and monitored in current-clamp mode to record action potentials. When the APD was stable for 2 min, cells were superfused with 185 nM C-PAF (Fig. 1), a concentration that elicited electrophysiological effects in 9 of 11 cells. C-PAF-evoked responses occurred after a delay (94 ± 21 s; range, 23–184 s) and typically included abnormal automaticity (Fig. 1; 110 s) leading to a maintained depolariza-

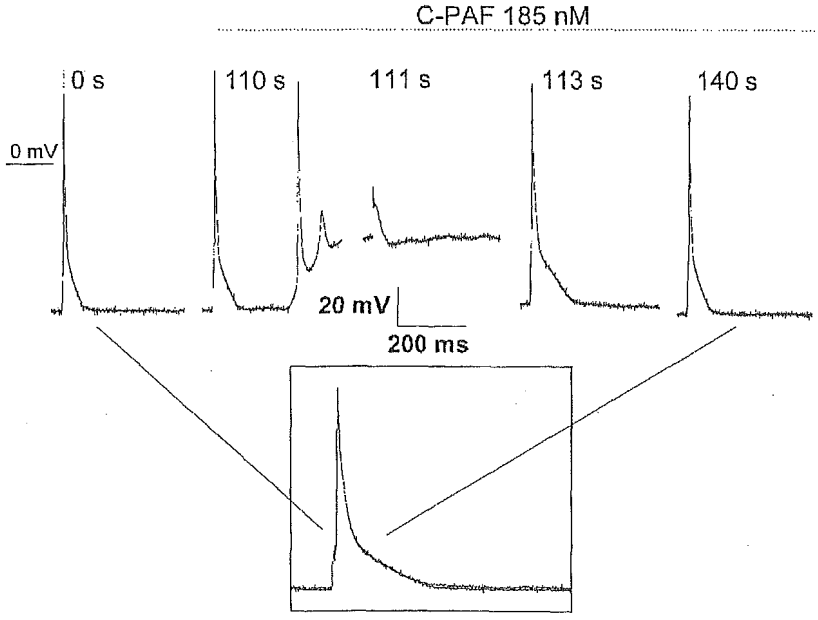

Fig. 1. Carbamyl-platelet-activating factor (C-PAF) alters normal action potentials in mouse ventricular myocytes. Paced action potentials (cycle length, 1,000 ms) were recorded in current-clamp mode under control conditions (0 s) and after perfusion of C-PAF (185 nM). After a delay, C-PAF caused abnormal automaticity (110 s) and sustained depolarization (111 s). The action potential progressively shortened and normal rhythm was reestablished, indicating desensitization of the receptor in continuous presence of drug (113 and 140 s). *Inset*: traces during control perfusion and after recovery completely overlap. The data are derived from a single cell and are typical of 8 cells. The traces were recorded immediately before the application of C-PAF (0 s) and 110, 111, 113, and 140 s after C-PAF application.

tion (Fig. 1; 111 s). In eight of nine cells, alteration of the membrane potential slowly returned to normal, presumably due to receptor desensitization, and after 3 min of agonist perfusion was indistinguishable from that of controls (Fig. 1, *inset*).

C-PAF decreases an outward current that is K^+ selective and carried by TASK-1. Cells were held at −10 mV, and total steady-state membrane currents were measured. The mean holding current was 133 ± 12 pA (n = 24). WT myocytes responded to C-PAF with decreased net outward current that often began to reverse during the perfusion and recovered completely after washout (Fig. 2*A*). Because a depolarizing shift in steady-state current can be caused by increased inward currents or decreased outward currents, we determined how C-PAF affected conductance. When a +10-mV step was applied during control and agonist superfusion, we found that C-PAF decreased conductance 17.5 ± 3.9% (n = 5, $P < 0.05$), indicating that the lipid inhibits outward currents. The main conductance maintaining resting potential in the ventricle is I_{K1}; therefore, we tested whether this inwardly rectifying K^+ current was involved in the action of C-PAF. Cs^+ (5 mM), which largely blocks I_{K1} under these conditions (data not shown), did not reduce the C-PAF-sensitive current in cells held at −70 mV. The average C-PAF-sensitive current density was 0.047 ± 0.01 pA/pF in control cells compared with 0.047 ± 0.03 pA/pF in cells in the presence of Cs^+ (n = 6). By extending the voltage-clamp study to other potentials, we obtained a nearly linear current-voltage relation for the C-PAF difference current (Fig. 2*B*, ■). In KO myocytes, the C-PAF-sensitive current was absent at all potentials tested (Fig. 2*B*, ●).

We did not observe a clear reversal potential in physiological K^+ over the voltage range tested. Therefore, we conducted additional experiments in elevated extracellular K^+ [50 mM K^+, with Na^+ reduced to 100 mM, plus 5 mM Cs^+ and 1 mM tetraethylammonium ion (TEA^+)] designed to measure the reversal potential of the C-PAF-sensitive current. In elevated extracellular K^+, our results show a weakly outward rectifying current with a current-voltage relation that is consistent with that of a predominantly K^+-selective channel (Fig. 2*C*). The calculated K^+ equilibrium potential for these recording conditions is −27.6 mV, and the observed reversal for the C-PAF-sensitive current occurred at −20.4 ± 3 mV (n = 5).

The C-PAF-sensitive current was blocked by the PAFR antagonist CV-6209 (100 nM; Fig. 3). The lack of a C-PAF-dependent response in the presence of CV-6209 was identical to the results obtained in myocytes derived from KO mice (Fig. 3). Taken together, these results confirm that the C-PAF effect is mediated by the PAFR and involves inhibition of an outward K^+ current distinct from I_{K1}.

These characteristics of the C-PAF-sensitive current suggested that it may be mediated by a member of the "two-pore domain" K^+ channel family (13). TASK-1 is a member of this family that is expressed in the mammalian heart (9, 10, 13, 14). In heterologous expression

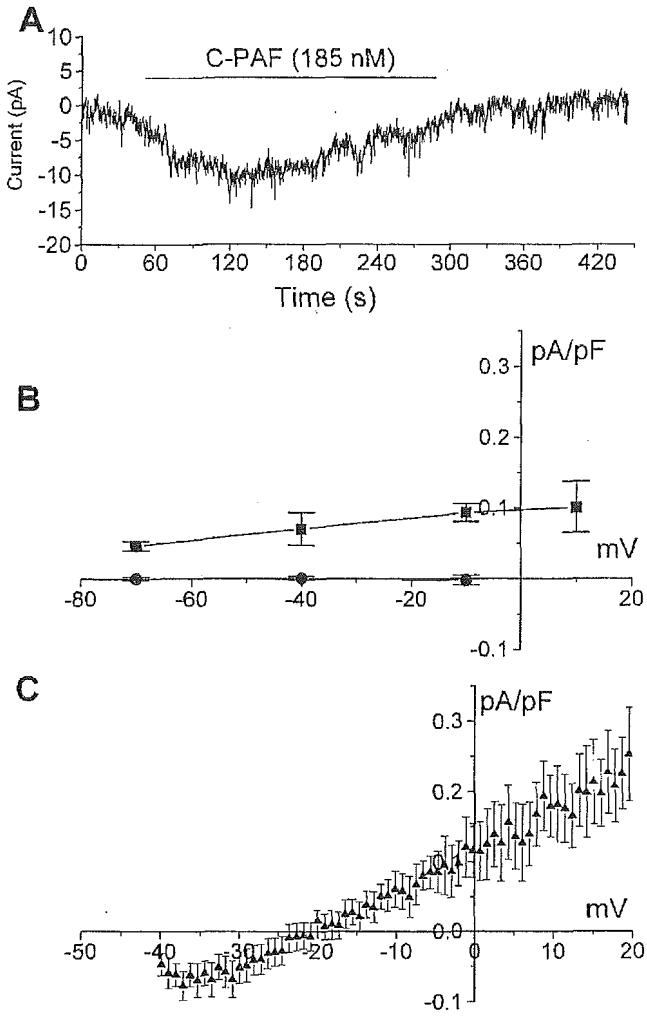

Fig. 2. Application of C-PAF causes a depolarizing shift in net membrane current in wild-type (WT) but not in knockout (KO) myocytes. Superfusion of C-PAF (185 nM) caused a transient decrease in the net outward current in a WT myocyte held at −10 mV (*A*). In this trace, the baseline outward holding current was adjusted to zero to illustrate the C-PAF-sensitive current. The spontaneous reversal of the C-PAF effect probably indicates desensitization of the PAF receptor (PAFR). The current (*I*)-voltage (*V*) relation of the C-PAF difference current (control minus C-PAF) is plotted as a net outward current over a range of potentials in WT myocytes (*B*, ■). In KO myocytes (●), no C-PAF-sensitive current was detected at all potentials tested. Each data point is the mean ± SE of data from at least 4 cells at each potential. The *I-V* relation was also measured using a ramp protocol in high extracellular K^+ (50 mM) plus Cs^+ (5 mM) and tetraethylammonium ion (1 mM) to permit determination of the reversal potential (*C*). Each data point is the mean ± SE of data from at least 5 cells from 2 animals.

systems, this channel is outwardly rectifying and is blocked by H^+, Ba^{2+}, Zn^{2+}, and anandamide, an endogenous cannabinoid receptor ligand (9, 10, 13, 14, 16, 18, 24). Consistent with this, in isolated myocytes, when the external pH was lowered to 6.4 or when Ba^{2+} (3 mM) or Zn^{2+} (3 mM) was present, the C-PAF-sensitive current was significantly reduced (Fig. 4). Methanandamide (10 μM), a stable analog of anandamide, also inhibited the C-PAF-sensitive current (Fig. 4). In contrast, anandamide inhibition was only significant in the presence of ATFK (10 μM), an inhibitor of

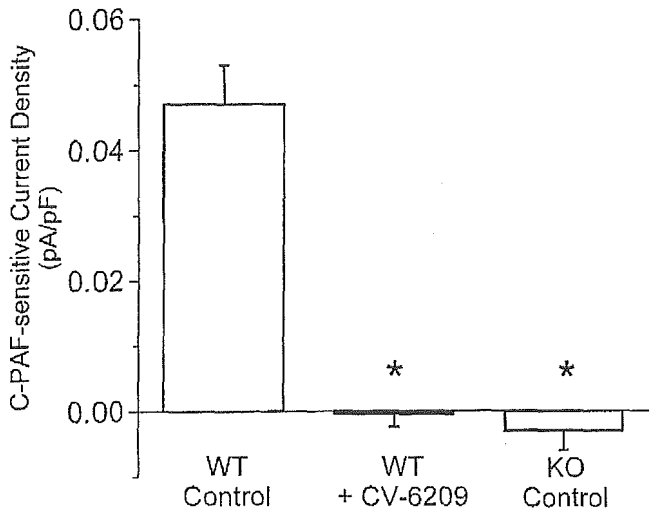

Fig. 3. The C-PAF-sensitive current is receptor mediated. The C-PAF-sensitive current was measured in WT myocytes held at −70 mV under various conditions. The current under control conditions in WT myocytes disappeared in the presence of the PAFR antagonist CV-6209 (100 nM, n = 5). There was no C-PAF-sensitive current detected in myocytes from KO mice (n = 3). *P < 0.01.

anandamide hydrolysis (Fig. 4), suggesting rapid metabolism of anandamide by ventricular myocytes. ATFK alone had no effect (data not shown).

CHO cells expressing TASK-1 exhibited a large outwardly rectifying current that was pH sensitive. The mean current-voltage relation at alkaline and acidic pH is shown in Fig. 5, *left*, and demonstrates that the reduction of the external pH to 6 completely eliminated the outwardly rectifying current. Mean current density at +30 mV in cells expressing TASK-1 was 26 pA/pF compared with 0.6 pA/pF for nontransfected cells. When TASK-1-transfected CHO cells were superfused with C-PAF (185 nM), the expressed current was reduced (Fig. 5, *right*), demonstrating the inhibitory effect of C-PAF on TASK-1-dependent current.

If both C-PAF and methanandamide block TASK-1, then methanandamide itself should cause a decreased net outward current. Thus the methanandamide-sensitive current was measured (Fig. 6). Because this current is comparable to the C-PAF-sensitive current, we also asked whether the methanandamide-sensitive current was mediated by the PAFR and found that the lipid was fully effective in the presence of the PAFR antagonist CV-6209 or when applied to myocytes from KO mice (Fig. 6). Thus the effect of methanandamide is not mediated by the PAFR.

C-PAF action involves PKC-dependent block of TASK-1. In many cell types, PAF initiates an intracellular pathway that results in activation of PKC (1, 17, 19, 23). To determine whether C-PAF initiates this cascade in ventricular myocytes, we incubated cells with BIM I, a selective PKC inhibitor (25) [inhibitory constant, 14 nM], before applying C-PAF. The C-PAF-sensitive current was blocked in a dose-dependent manner (Fig. 7, *A* and *B*) by BIM I but was not altered by the addition of an inactive analog, BIM V. The inhibition occurred in a voltage-independent manner (Fig. 7*C*).

We then asked whether the methanandamide-sensitive current also required PKC activity. BIM I (100 nM) significantly reduced the methanandamide-sensi-

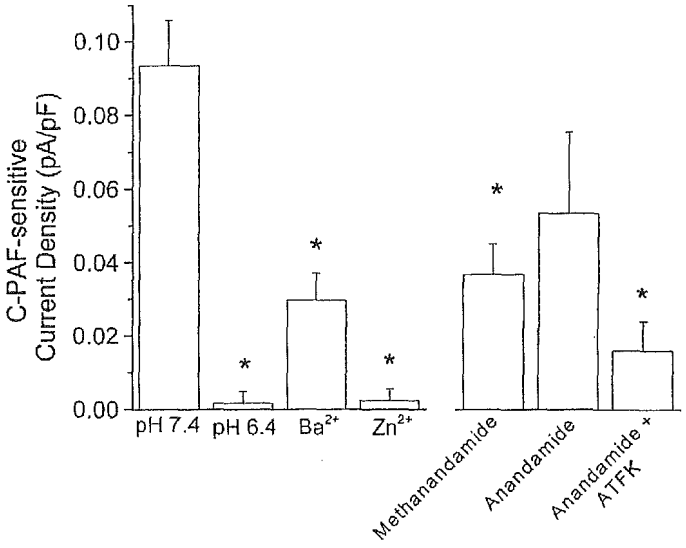

Fig. 4. Block of the TWIK-related acid-sensitive K^+ background channel (TASK-1) decreases the C-PAF-sensitive steady-state current. WT myocytes were held at −10 mV, and the C-PAF-sensitive current was measured at pH 7.4 (n = 25). The change in net current elicited by C-PAF (185 nM) was significantly decreased in the presence of Tyrode buffer at pH 6.4 (n = 6), Ba^{2+} (3 mM, n = 6), or Zn^{2+} (3 mM, n = 8). The stable anandamide analog methanandamide (10 μM, n = 12) also significantly reduced the C-PAF-sensitive current, as did anandamide in the presence of arachidonyltrifluoromethyl ketone (ATFK), a drug that inhibits anandamide metabolism (10 μM, n = 8). Anandamide alone did not significantly inhibit the current (10 μM, n = 5) due to its rapid metabolic inactivation. *P < 0.05 compared with control at pH 7.4.

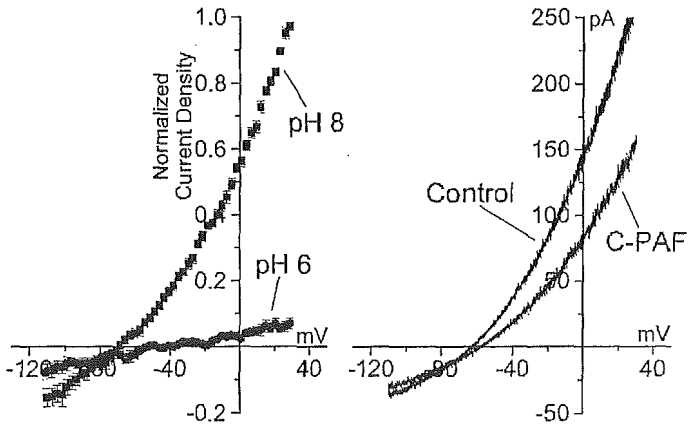

Fig. 5. TASK-1 heterologously expressed in CHO cells is sensitive to pH and to C-PAF. Net steady-state current was measured by a ramp clamp under alkaline (pH 8) and acidic (pH 6) conditions, demonstrating the pH sensitivity of the expressed TASK-1 current. The *I-V* relation of each cell was normalized to the current at 30 mV to correct for cell-to-cell variability in expression levels, and the mean normalized current density was plotted (*left*, n = 13). In CHO cells exposed to C-PAF (185 nM), the expressed TASK-1 current was decreased (*right*). Representative *I-V* relations before (control) and during drug treatment (C-PAF) were compared. This result is representative of 8 cells. On average, the *I-V* relation returned to within 5% of control value after washout of C-PAF.

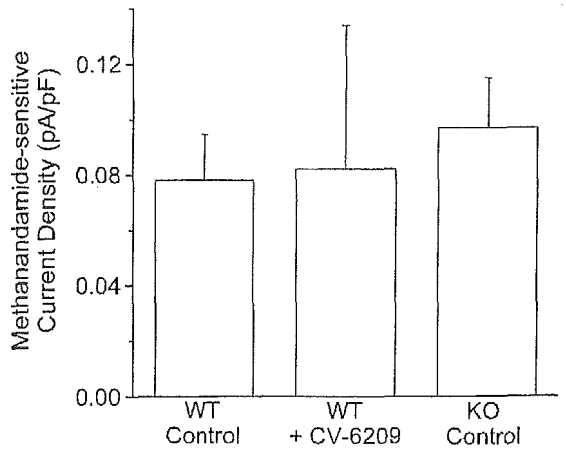

Fig. 6. The methanandamide-sensitive current is independent of the PAFR. WT cells held at −10 mV were superfused with methanandamide (10 μM), and the methanandamide-sensitive current was measured (WT control, $n = 6$). The methanandamide-sensitive current did not differ from control when WT cells were incubated with the PAFR antagonist CV-6209 (100 nM, $n = 3$) or in myocytes derived from PAFR knockout mice (KO control, $n = 6$).

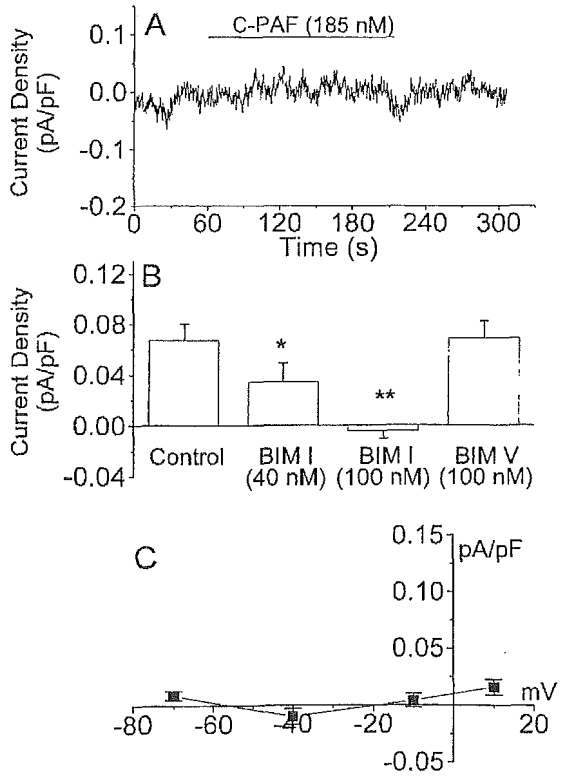

Fig. 7. The C-PAF-sensitive current is blocked by inhibition of protein kinase C (PKC). The C-PAF-sensitive current was completely blocked in myocytes (held at −10 mV) exposed to bisindolylmaleimide I (BIM I), a specific PKC inhibitor (100 nM; *A*). In this trace, the baseline holding current was adjusted to zero to illustrate the absence of a C-PAF-sensitive current. BIM I-mediated inhibition of the C-PAF-sensitive current is dose dependent (*B*; 40 nM, $n = 7$, and 100 nM, $n = 11$). An inactive BIM I analog, BIM V, does not block the C-PAF-sensitive current (*B*; $n = 10$). The inhibition of the C-PAF-sensitive current by BIM I is independent of voltage (*C*; 100 nM BIM, n = at least 4 for each data point). $^*P < 0.05$ and $^{**}P < 0.001$ vs. control.

tive current in WT myocytes ($P < 0.05$, $n = 5$; data not shown).

C-PAF and methanandamide induce spontaneous activity in quiescent myocytes. Because C-PAF and methanandamide affect net steady-state current at voltages near the resting potential, we asked whether electrophysiological effects occurred independent of pacing. Membrane potential was recorded from myocytes that remained quiescent for at least 2 min. Every WT quiescent myocyte tested was sensitive to C-PAF superfusion (11 of 11 cells; Fig. 8*A*), typically responding with an action potential that arrested in the plateau phase (Fig. 8*A*, *inset*), and exhibited many small fluctuations of the membrane potential and EAD. Eventually, the membrane repolarized. The duration of the effect was variable, but its appearance always followed an initial delay (96 ± 11 s). In contrast, when C-PAF was applied to ventricular myocytes isolated from PAFR KO mice, there was no response in most of the cells (7 of 9 cells;

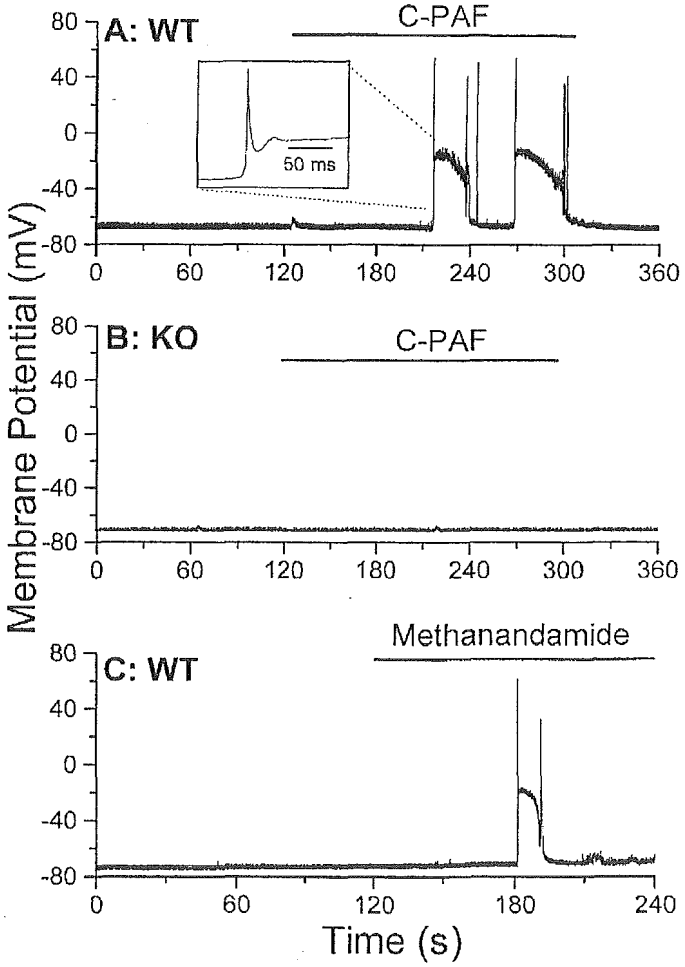

Fig. 8. C-PAF and methanadamide elicit spontaneous activity in quiescent WT myocytes. Quiescent myocytes from WT and KO mice were studied in current-clamp mode. C-PAF (185 nM) application elicited spontaneous activity in WT (*A*) but not KO myocytes (*B*). Superfusion of methanandamide (10 μM) over WT myocytes caused the same effect as C-PAF (*C*). There was no measurable change in the resting potential before impulse initiation. These recordings are typical of 11 cells for *A*, 7 cells for *B*, and 7 cells for *C*.

Fig. 8*B*). The responsiveness of WT and KO myocytes to C-PAF differed significantly ($P < 0.01$, $\chi^2 = 9.96$), although their resting potentials did not (-70.6 ± 1.1 vs. -71.3 ± 1.5 mV). Finally, six of eight quiescent WT cells failed to respond to C-PAF (185 nM) after BIM I treatment (100 nM). A comparison of BIM-treated to control myocytes indicated a significant reduction in susceptibility to spontaneous activity ($P < 0.01$, $\chi^2 = 8.84$).

If the decrease in outward current caused by blocking the TASK-1 channel is related to the arrhythmogenic effects of C-PAF, application of a TASK-1 inhibitor in current-clamp mode should mimic the effects of C-PAF and evoke spontaneous activity. Accordingly, when methanandamide was applied to quiescent WT myocytes, spontaneous action potentials were observed (7 of 12 cells; Fig. 8*C*). Statistical analysis showed no difference in the occurrence of spontaneous activity during methanandamide compared with C-PAF superfusion.

DISCUSSION

Inflammatory products released by PMNL can have negative effects on cardiac function and the survival of areas at risk after periods of ischemia and reperfusion (15). Our earlier studies in isolated canine ventricular myocytes (4) demonstrated that PAF, a PMNL-derived inflammatory lipid, could alter action potentials by prolongation of the APD, EADs, and arrest at the plateau. The present study demonstrates that in murine ventricular myocytes, C-PAF also triggers a series of alterations in action potentials, including spontaneous beats, EADs, and prolonged depolarization similar to those observed in canine myocytes (4, 5). This supports the validity of the mouse as a model in which to study the molecular basis of the arrhythmogenic effect of PAF.

We measured changes in the membrane potential, spontaneous activity, and in specific ion currents in myocytes as they were exposed to C-PAF. This lipid causes a small change in net current that develops over the first minute after application. Changes in the action potential (or appearance of spontaneous action potentials in quiescent cells) lag behind the peak current by ~20 s (at −70 mV, the C-PAF-sensitive current peaked by 74 ± 13 s). The generation of spontaneous activity in quiescent myocytes implies that changes in membrane potential are not strictly dependent on the stimulus or alterations in active currents but rather that it is likely that the agonist perturbs the balance among those currents active at the resting membrane potential. Voltage-clamp experiments measuring changes in conductance indicate that C-PAF effects are dependent on a decrease in outward currents. In addition, the C-PAF-sensitive current, measured in elevated K^+, showed weak outward rectification and had a reversal potential close to the calculated K^+ equilibrium potential. These data indicate that the C-PAF-sensitive current is largely carried by K^+.

Because experiments utilizing Cs^+ argue against the involvement of I_{K1} in the ionic mechanism underlying the PAF-sensitive current, our attention shifted to other K^+ channels that are active at rest. The two-pore domain K^+ channels (13) are voltage- and time-independent background channels having characteristics similar to the channel responsible for the C-PAF-sensitive current. Within this family, TASK-1 [also referred to as cTBAK-1 (9) and Kcnk3 (14)] is expressed in the heart (10). TASK-1 is sensitive to small variations in external pH and is almost completely inhibited at pH 6.4. It is also blocked by Ba^{2+} or Zn^{2+} and by the putative endogenous lipid ligand of the cannabinoid receptors anandamide (16). The C-PAF-sensitive current in murine ventricular myocytes was sensitive to all these interventions, suggesting that C-PAF-mediated effects are associated with inhibition of TASK-1 or a closely related channel. Confirmation that the TASK-1 channel is sensitive to C-PAF was obtained by expressing TASK-1 in CHO cells. When TASK-1-expressing CHO cells were superfused with C-PAF, the expressed current was reduced.

Because our data suggested that the C-PAF-sensitive current is due to TASK-1 blockade, we reasoned that anandamide treatment might prevent myocytes from responding to C-PAF. In fact, both anandamide in the presence of ATFK, an inhibitor of anandamide hydrolysis, and its nonhydrolyzable analog, methanandamide, significantly reduced the C-PAF effect, confirming our hypothesis. It follows that if C-PAF and methanandamide both inhibit TASK-1 and if this is the ionic basis for the C-PAF-sensitive effects, methanandamide should induce similar changes in myocyte physiology. As predicted, methanandamide caused both a decrease in net outward current and an increase in spontaneous activity in quiescent myocytes. Therefore, we conclude that both C-PAF and methanandamide exert their biological effects at least in part by inhibiting TASK-1 or a closely related channel.

In a heterologous expression system, Maingret et al. (16) found that anandamide inhibition of TASK-1 was not mediated by the known cannabinoid receptors, and, because the drug was effective on excised macropatches, they concluded that the lipid interacted directly with the channel. PAF, in contrast, is known to activate cells through a G protein-linked receptor that initiates a signaling cascade involving activation of phospholipase C, generating inositol phosphates and elevating intracellular calcium and diacylglycerol, ultimately activating PKC (1, 8, 17, 19). In our studies, the effect of C-PAF is clearly mediated by the PAFR because its activity can be blocked by the antagonist CV-6209 and is absent in myocytes derived from mice in which the PAFR has been genetically deleted. In addition, we found that inhibition of PKC blocked the C-PAF-sensitive current. Although several reports suggest that TASK-1 is insensitive to PKC activators (3, 12), Lopes et al. (14) found that phorbol 12-myristate 13-acetate causes a slowly developing block of TASK-1 current in an oocyte expression system. This further supports our hypothesis that C-PAF activity is

mediated by activation of PKC-dependent phosphorylation, and, although it does not resolve the mechanism behind the somewhat unexpected time course of the effect, it is entirely consistent with our findings.

Interestingly, PKC inhibition also reduced the methanandamide-sensitive current, suggesting that the two lipids share overlapping intracellular signaling pathways. Therefore, we tested whether methanandamide required the PAFR for its activity and found that it was fully functional in the presence of CV-6209 and in myocytes derived from KO mice. These data suggest that the methanandamide effect is dependent, at least in part, on PKC activation. Alternatively, the block of the TASK-1 channel by methanandamide may require a basal phosphorylation of the channel itself or an accessory protein and thus ultimately depends on, but is not mediated by, PKC. Such a scenario was recently described for a similar effect of anandamide on the VR_1 vanilloid receptor, a nonselective cation channel. In this case, activation of the receptor by anandamide was significantly enhanced when the channel had been phosphorylated by PKC, and anandamide itself stimulated PKC (21).

These results suggest, for the first time, a role for the TASK-1 channel in PAF-mediated arrhythmias. However, additional questions remain. While block of TASK-1 channels could contribute to a longer APD and subsequent EADs, this does not preclude additional effects on other currents active during the action potential plateau, including Ca^{2+}, Na^+, and the delayed rectifier currents. In addition, the mechanism by which TASK-1 blockade might lead to initiation of spontaneous activity in a quiescent myocyte is not clear, because no measurable change in membrane potential was observed immediately preceding initiation of activity induced by either C-PAF or methanandamide. Additional mechanisms, either secondary to the block of TASK-1 or independent of this action, may occur after exposure to PAF. The murine model, and its amenability to genetic manipulations, should prove useful in the ultimate resolution of these remaining questions.

The authors thank Irina Voloshyna and Patricia McLaughlin for excellent technical assistance and Dr. Michael R. Rosen for critical comments on the manuscript.

This work was supported by National Heart, Lung, and Blood Institute Grant HL-56140 and by a Servier Strategic Alliance.

REFERENCES

1. **Chao W and Olson MS.** Platelet-activating factor: receptors and signal transduction. *Biochem J* 292: 617–629, 1993.
2. **DiFrancesco D, Ferroni A, Mazzanti M, and Tromba C.** Properties of the hyperpolarizing-activated current (i_f) in cells isolated from the rabbit sino-atrial node. *J Physiol (Lond)* 377: 61–88, 1986.
3. **Duprat F, Lesage F, Fink M, Reyes R, Heurteaux C, and Lazdunski M.** TASK, a human background K^+ channel to sense external pH variations near physiological pH. *EMBO J* 16: 5464–5471, 1997.
4. **Hoffman BF, Feinmark SJ, and Guo SD.** Electrophysiologic effects of interactions between activated canine neutrophils and cardiac myocytes. *J Cardiovasc Electrophysiol* 8: 679–687, 1997.
5. **Hoffman BF, Guo SD, and Feinmark SJ.** Arrhythmias caused by platelet activating factor. *J Cardiovasc Electrophysiol* 7: 120–133, 1996.
6. **Ishii S, Kuwaki T, Nagase T, Maki K, Tashiro F, Sunaga S, Cao WH, Kume K, Fukuchi Y, Ikuta K, Miyazaki J, Kumada M, and Shimizu T.** Impaired anaphylactic responses with intact sensitivity to endotoxin in mice lacking a platelet-activating factor receptor. *J Exp Med* 187: 1779–1788, 1998.
7. **Ishii S, Nagase T, Tashiro F, Ikuta K, Sato S, Waga I, Kume K, Miyazaki J, and Shimizu T.** Bronchial hyperreactivity, increased endotoxin lethality and melanocytic tumorigenesis in transgenic mice overexpressing platelet-activating factor receptor. *EMBO J* 16: 133–142, 1997.
8. **Ishii S and Shimizu T.** Platelet-activating factor (PAF) receptor and genetically engineered PAF receptor mutant mice. *Prog Lipid Res* 39: 41–82, 2000.
9. **Kim D, Fujita A, Horio Y, and Kurachi Y.** Cloning and functional expression of a novel cardiac two-pore background K^+ channel (cTBAK-1). *Circ Res* 82: 513–518, 1998.
10. **Kim Y, Bang H, and Kim D.** TBAK-1 and TASK-1, two-pore K^+ channel subunits: kinetic properties and expression in rat heart. *Am J Physiol Heart Circ Physiol* 277: H1669–H1678, 1999.
11. **Kuznetsov V, Pak E, Robinson RB, and Steinberg SF.** β_2-Adrenergic receptor actions in neonatal and adult rat ventricular myocytes. *Circ Res* 76: 40–52, 1995.
12. **Leonoudakis D, Gray AT, Winegar BD, Kindler CH, Harada M, Taylor DM, Chavez RA, Forsayeth JR, and Yost CS.** An open rectifier potassium channel with two pore domains in tandem cloned from rat cerebellum. *J Neurosci* 18: 868–877, 1998.
13. **Lesage F and Lazdunski M.** Molecular and functional properties of two-pore-domain potassium channels. *Am J Physiol Renal Physiol* 279: F793–F801, 2000.
14. **Lopes CMB, Gallagher PG, Buck ME, Butler MH, and Goldstein SAN.** Proton block and voltage gating are potassium-dependent in the cardiac leak channel Kcnk3. *J Biol Chem* 275: 16969–16978, 2000.
15. **Lucchesi BR and Mullane KM.** Leukocytes and ischemia-induced myocardial injury. *Annu Rev Pharmacol Toxicol* 26: 201–224, 1986.
16. **Maingret F, Patel AJ, Lazdunski M, and Honore E.** The endocannabinoid anandamide is a direct and selective blocker of the background K^+ channel TASK-1. *EMBO J* 20: 47–54, 2001.
17. **Massey CV, Kohout TA, Gaa ST, Lederer WJ, and Rogers TB.** Molecular and cellular actions of platelet-activating factor in rat heart cells. *J Clin Invest* 88: 2106–2116, 1991.
18. **Millar JA, Barratt L, Southan AP, Page KM, Fyffe R, Robertson B, and Mathie A.** A functional role for the two-pore domain potassium channel TASK-1 in cerebellar granule neurons. *Proc Natl Acad Sci USA* 97: 3614–3618, 2000.
19. **Montrucchio G, Alloatti G, and Camussi G.** Role of platelet-activating factor in cardiovascular pathophysiology. *Physiol Rev* 80: 1669–1699, 2000.
20. **Mullane KM, Read N, Salmon JA, and Moncada S.** Role of leukocytes in acute myocardial infarction in anesthetized dogs: relationship to myocardial salvage by anti-inflammatory drugs. *J Pharmacol Exp Ther* 228: 510–522, 1984.
21. **Premkumar L and Ahern GP.** Induction of vanilloid receptor channel activity by protein kinase C. *Nature* 408: 985–990, 2000.
22. **Romson JL, Hook BG, Kunkel SL, Abrams GD, Schork MA, and Lucchesi BR.** Reduction of the extent of ischemic myocardial injury by neutrophil depletion in the dog. *Circulation* 67: 1016–1023, 1983.
23. **Shukla SD.** Platelet-activating factor receptor and signal transduction mechanisms. *FASEB J* 6: 2296–2301, 1992.
24. **Talley E, Lei Q, Sirois J, and Bayliss D.** TASK-1, a two-pore domain K^+ channel, is modulated by multiple neurotransmitters in motoneurons. *Neuron* 25: 399–410, 2000.
25. **Toullec D, Pianetti P, Coste H, Bellevergue P, Grand-Perret T, Ajakane M, Baudet V, Boissin P, Boursier E, and Loriolle F.** The bisindolylmaleimide GF 109203X is a potent and selective inhibitor of protein kinase C. *J Biol Chem* 266: 15771–15781, 1991.
26. **Wahler GM, Coyle DE, and Sperelakis N.** Effects of platelet-activating factor on single potassium channel currents in guinea pig ventricular myocytes. *Mol Cell Biochem* 93: 69–76, 1990.

THE JOURNAL OF BIOLOGICAL CHEMISTRY
Vol. 277, No. 21, Issue of May 24, pp. 18763–18768, 2002
Printed in U.S.A.
© 2002 by The American Society for Biochemistry and Molecular Biology, Inc.

Characterization of Mouse Cysteinyl Leukotriene Receptors mCysLT$_1$ and mCysLT$_2$

DIFFERENTIAL PHARMACOLOGICAL PROPERTIES AND TISSUE DISTRIBUTION*

Received for publication, October 1, 2001, and in revised form, February 15, 2002
Published, JBC Papers in Press, February 19, 2002, DOI 10.1074/jbc.M109447200

Hideaki Ogasawara‡§, Satoshi Ishii‡§, Takehiko Yokomizo‡§, Takashi Kakinuma¶, Mayumi Komine¶, Kunihiko Tamaki¶, Takao Shimizu‡§‖, and Takashi Izumi§**

*From the Departments of ‡Biochemistry and Molecular Biology and ¶Dermatology, Faculty of Medicine, The University of Tokyo, Bunkyo-ku, Tokyo 113-0033, §CREST of Japan Science and Technology Corporation, Bunkyo-ku, Tokyo 113-0033, and the **Department of Biochemistry, Gunma University School of Medicine, Maebashi, Gunma 371-8511, Japan*

Cysteinyl leukotrienes (LTs) are important proinflammatory mediators. Their precise roles in mice need to be elucidated to interpret mouse models of inflammatory diseases. For this purpose, we cloned and characterized mouse receptors for cysteinyl LTs, mCysLT$_1$ and mCysLT$_2$. mCysLT$_1$ and mCysLT$_2$ were composed of 339 amino acids with 87.3% identity and 309 amino acids with 73.4% identity to human orthologues, respectively. A pharmacological difference was noted between mouse and human CysLT$_2$. Pranlukast, a specific inhibitor for human CysLT$_1$, antagonized mCysLT$_2$ responses as determined by Ca^{2+} elevation and receptor-induced promoter activation. The mRNA expressions of both mCysLTs were higher in C57BL/6 mice than in 129 mice. mCysLT$_1$ mRNA was expressed mainly in skin, lung, and small intestine. mCysLT$_2$ was seen more ubiquitously with high expressions in spleen, lung, and small intestine. By *in situ* hybridization we demonstrated for the first time that mCysLT$_1$ and mCysLT$_2$ were expressed in subcutaneous fibroblasts. The different pharmacological characteristics of CysLT$_2$ between human and mouse and the different distributions of CysLTs between mouse strains suggest that careful choice and interpretation are necessary for a study of CysLTs using animal models.

Cysteinyl leukotrienes (LTs)[1] including LTC$_4$, LTD$_4$, and LTE$_4$ are inflammatory mediators previously known as SRS-A (slow reacting substances of anaphylaxis) (1–4). They are produced by LTC$_4$ synthase from the biologically inactive precursor LTA$_4$, a product of 5-lipoxygenation of arachidonic acid (5–7). LTC$_4$ synthase is expressed in inflammatory cells including mast cells, eosinophils, basophils, and monocytes/macrophages (7). The cysteinyl LTs are potent bronchoconstrictors and macrophage activators, and have been identified in urine and tissues in asthmatic patients (8–10). At least two cysteinyl LT receptors (CysLT$_1$ and CysLT$_2$) have been defined pharmacologically as G protein-coupled receptors. Most of the biological reactions of cysteinyl LTs including bronchospasm, plasma exudation, vasoconstriction, mucus secretion, and eosinophil recruitment are mediated through interaction with CysLT$_1$ (11). CysLT$_1$ antagonists, montelukast (Singulair™) (12, 13), zafirlukast (Accolate™) (14), and pranlukast (Onon™) (15) are currently used clinically for the treatment of bronchial asthma and allergic rhinitis. Human CysLT$_1$, human CysLT$_2$, and mouse CysLT$_1$ were recently cloned and characterized (16–21). Human CysLT$_1$ mRNA was detected in airway smooth muscle cells, tissue macrophages, monocytes, and eosinophils (16, 17). Human CysLT$_2$ mRNA was prominently expressed in lung macrophages, airway smooth muscle, cardiac Purkinje cells, adrenal medulla cells, peripheral blood leukocytes, placenta, spleen, and brain (18–20).

Ovalbumin sensitization and aerosol challenge in mice elicits release of LTB$_4$ and LTC$_4$ into bronchoalveolar lavage fluid, eosinophilia in the mucosa and the bronchoalveolar lavage fluid, and increased airway reactivity to methacholine (22). Although cysteinyl LTs are not established as bronchoconstrictors in mice, MK-571, a CysLT$_1$-selective antagonist, inhibits eosinophilia, bronchial hyperreactivity, and microvascular leakage of mice (23), suggesting a contribution of cysteinyl LTs in these processes. We cloned and characterized the mouse CysLT$_1$ (mCysLT$_1$) and CysLT$_2$ (mCysLT$_2$) to better study the roles of cysteinyl LTs in animal models of diseases.

MATERIALS AND METHODS

Antagonists—Pranlukast was a generous gift from Ono Pharmaceutical Co. (Osaka, Japan). MK-571 and BAY u9773 were purchased from BIOMOL Research Laboratories (Plymouth Meeting, PA). Pranlukast and MK-571 were dissolved in 100% ethanol to make 10 mM stock solutions.

Cloning and Expression of mCysLT$_1$ and mCysLT$_2$—A mouse genome library (129 inbred strain) in λFix II vector (Stratagene, La Jolla, CA) was screened with [α-^{32}P]dCTP-labeled partial open reading frame (ORF) of human CysLT$_1$ (581 nucleotides), and a clone was isolated. The CysLT$_1$ ORF from C57BL/6 was obtained by PCR with a genome template using sense (5′-ATTCCTGGAGAACATGAATGG-3′) and antisense (5′-CATTGTTCTGCACTGTAGATGAG-3′) primers. A mouse expressed sequence tag clone with 88.4% identity in cDNA sequence to the human CysLT$_1$ was found during a routine BLAST search of the NCBI data base (GenBank™ accession number AI506060), and it was purchased from Genome Systems (St. Louis, MO). These three clones were sequenced using an automated DNA sequencer 373A (Applied Biosystems, Foster City, CA) and found to be completely identical. The ORF of the expressed sequence tag clone was amplified by PCR with

* The work was supported in part by Grants-in-aid from the Ministry of Education, Culture, Sports, Science and Technology of Japan and grants from the Yamanouchi Foundation for Metabolic Disorders and the ONO Medical Research Foundation. The costs of publication of this article were defrayed in part by the payment of page charges. This article must therefore be hereby marked "*advertisement*" in accordance with 18 U.S.C. Section 1734 solely to indicate this fact.

The nucleotide sequence(s) reported in this paper has been submitted to the GenBank™/EBI Data Bank with accession number(s) AB044087 and AB058930.

‖ To whom correspondence should be addressed. Tel.: 81-3-5802-2925; Fax: 81-3-3813-8732; E-mail: tshimizu@m.u-tokyo.ac.jp.

[1] The abbreviations used are: LT, leukotriene; CHO, Chinese hamster ovary; FCS, fetal calf serum; G3PDH, glyceraldehyde-3-phosphate dehydrogenase; HEK, human embryonic kidney; ORF, open reading frame; PBS, phosphate-buffered saline; m, mouse; AM, acetoxymethyl; TM, transmembrane domain.

A

```
                                                  I                                  II
mCysLT1    1' MNGTENLTT--SLINNTCHDTIDEFRNQVYSTMYSVISVVGFFGNSFVLYVLIKTYHEKSAFQVYMINLAIADLLCVCTLPLRVVYYVHKGKWLFGDFLCRL
                *   *   *   *         **..*... *...* .*    * .**.* .**...*...... .*.*.***..*.* ..***.*. ** . ..*.***. **.
mCysLT2    1' M---EVTGTPSS--YSNRNCTIENFKKEFYPIIYLIIFFWGALGNGFSIYVFLQTCKKSTSVNVFMLNLATSDFLFISTLPFRADYYFRGSNWIFGDLACRV

                          III                                IV
mCysLT1  101' TTYALYVNLYCSIFFMTAMSFFRCVAIVFPVQNINLVTQKKARFVCIGIWIFVILTSSPFLMYKSYQDEKNNTKCFEPPQNNQAKKYVLILHYVSLFFGF
                .*.****.* **.*.*..*  * .*.* * . ..... ..*...* **.* *..**..*. .. ....* ..*.*   . *  * .**..... **
mCysLT2   98' MSYSLYVNMYTSIYFLTVLSVVRFLATVHPFRMFHVTSVRSAWILCGIIWVF-IMASSALLLVNGQEEKDNIISCLE--LSPQKFKSLLIMNHIAVAVGF

                V                                  VI                                VII
mCysLT1  201' IIPFVTIIVCYTMIILTLLKNTMKKNMP--SRRKAIGMIIVVTAAFLVSFMPYHIQRTIHLHLLHSETRPCDSVLRMQKSVVITLSLAASNCCFDPLLYFFS
                ..**.*...** .** .***... .. *  ..***.. *...  .**..*.*** ** ***.  .. .*..** .*..***..**.*.**.*.**.*.
mCysLT2  195' LLPFLTLTICYLLIIRILLKAEIPESGPRAAHRKALTTIVIAMITFLLCFLPYHALRT--LHLVTWDKDSCGDVL--HKATVITLTMAAANSCFNPFLYYFA

mCysLT1  301' GGNFRRRL-STFRKHSLSSMTYVPKKKASLPEKGEEICNE
                *.**. ** ..*.*  *
mCysLT2  293' GENFKARLRAIFSKVHL
```

B

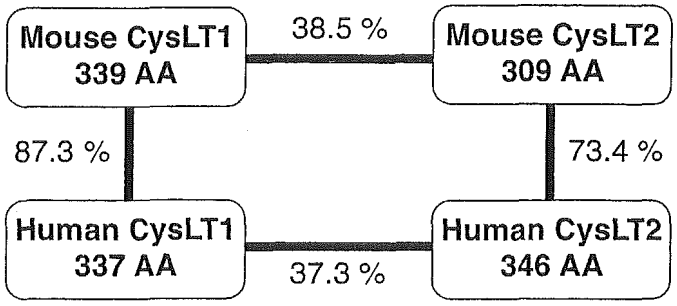

FIG. 1. **Amino acid sequence of mCysLT$_1$ and mCysLT$_2$.** *A*, structures of mCysLT$_1$ and mCysLT$_2$ are shown. The putative transmembrane segments I–VII of mCysLT$_1$ and mCysLT$_2$ are *underlined*. The *asterisks* indicate identical amino acids, and *dots* indicate similar amino acids. *B*, amino acid identities between mCysLT$_1$, mCysLT$_2$, human CysLT$_1$, and human CysLT$_2$ are shown. *AA*, amino acids.

sense (5′-CGGGATCCCGAATGGAACTGAAAATCTGAC-3′) and antisense (5′-GCTCTAGAGCTTATTCGTTACATATTTCTT-3′) primers, subcloned into a pGEM-T Easy Vector (Promega, Madison, WI), digested with restriction enzymes (*Bam*HI and *Xba*I), and subcloned again into an expression vector, pcDNA4HisMax (Invitrogen, Carlsbad, CA) to obtain pc4HM-mCysLT$_1$. For the cloning of a mouse CysLT$_2$ orthologue, the mouse genomic library in λFixII vector was screened by plaque hybridization using [α-^{32}P]dCTP-labeled full-length ORF of human CysLT$_2$ cDNA (19) as a probe. The fragments that hybridized to human CysLT$_2$ probe were sequenced as described above. The putative ORF was attached with an hemagglutinin tag at its N terminus and subcloned into an expression vector pcDNA3.1 (Invitrogen) between the *Kpn*I site and the *Xba*I site to obtain pc3.1-mCysLT$_2$. The CysLT$_2$ ORF from C57BL/6 was obtained by PCR with a genome template using primers designed from the 129 genome sequence.

Cell Culture and Transfection—HEK-293 cells and B103 cells were cultured in Dulbecco's modified Eagle's medium (Sigma) supplemented with 10% fetal calf serum (FCS; Sigma), 100 IU/ml penicillin, and 100 μg/ml streptomycin; PC12 cells in Dulbecco's modified Eagle's medium supplemented with 10% horse serum, 10% FCS, 100 IU/ml penicillin, and 100 μg/ml streptomycin; and CHO cells in Nutrient Mixture F-12 HAM (Sigma) supplemented with 10% FCS, 100 IU/ml penicillin, and 100 μg/ml streptomycin. Superfect (Qiagen, Valencia, CA) was used for the transfection of HEK-293 cells, B103 cells, and PC12 cells, and FuGENE 6 (Roche Molecular Biochemicals) was used for the transfection of CHO cells, according to the manufacturers' protocols. To obtain HEK-293 cells stably expressing mCysLT$_1$, the cells were transfected with pc4HM-mCysLT$_1$ and selected with 500 μg/ml Zeocin (Invitrogen). Two lines of the cells (named HEK 7-1 and HEK 7-3) were chosen by the increase of intracellular Ca^{2+} concentration ($[Ca^{2+}]_i$) in response to LTD_4 (see below) and maintained in Dulbecco's modified Eagle's medium with 10% FCS, 100 IU/ml penicillin, 100 μg/ml streptomycin, and 200 μg/ml Zeocin. The expression of mCysLT$_1$ was confirmed by Northern hybridization. HEK-293 cells transfected with the vector alone were also kept in a medium with Zeocin and used as a vector control. To obtain CHO cells stably expressing mCysLT$_2$, the cells were transfected with pc3.1-mCysLT$_2$ and selected with 1 mg/ml G418 (Invitrogen). Two lines of the cells (named CHO-7A1 and CHO-8B3) were chosen by Northern hybridization and maintained in F-12 with 10% FCS, 100 IU/ml penicillin, 100 μg/ml streptomycin, and 300 μg/ml G418. CHO cells transfected with the vector alone were also kept in a medium with G418 and used as a vector control.

Ca^{2+} Response Assay—The cells stably expressing mouse CysLTs were loaded with 3 μM Fura2-AM (Dojindo, Kumamoto, Japan) in a modified HEPES-Tyrode's bovine serum albumin buffer (25 mM Hepes-NaOH, pH 7.4, 140 mM NaCl, 2.7 mM KCl, 1.0 mM $CaCl_2$, 12 mM $NaHCO_3$, 5.6 mM D-glucose, 0.37 mM NaH_2PO_4, 0.49 mM $MgCl_2$, and 0.1% (w/v) bovine serum albumin (Wako, Osaka, Japan)) containing 0.01% Cremophor EL (Sigma) at 37 °C for 1 h. The cells were detached from dishes with PBS containing 2 mM EDTA, collected, centrifuged at 240 × *g* for 5 min in a 15-ml tube, and resuspended in the modified HEPES-Tyrode's bovine serum albumin buffer (2×10^6 cells/ml). The change in the fluorescence ratio (340 nm/380 nm) in response to LTs was monitored using a Ca^{2+} analyzer, CAF-100 (Jasco, Tokyo, Japan). $[Ca^{2+}]_i$ was estimated as described previously (24). A receptor antagonist was applied 5 min before stimulation with LTC_4 or LTD_4.

Reporter Gene Assay—We have recently established a zif268-driven promoter assay induced by receptor activation (25), and the original method was modified. Briefly, 1×10^4 B103 cells were seeded in collagen-coated 96-well microplates (Asahi Techno Glass, Tokyo, Japan) and transfected with 25 ng of pc4HM-mCysLT$_1$ or vector alone in combination with 150 ng of zif268-firefly luciferase/pGL2, which was a generous gift of Dr. T. Naito at Japan Tobacco Inc. (Tokyo, Japan). They were incubated for 48 h and treated with LTs in a serum-free medium. Receptor antagonists were applied 15 min before the stimulation. The cells were lysed after 4 h of incubation at 37 °C. Luciferase activity was determined by measuring luminescent signals using a luciferase reporter gene assay system, PICAGENE Dual Seapansy (Toyo Ink, Tokyo, Japan) and a Top Count luminescence counter (Packard, Meriden, CT). For the assay of CysLT$_2$, 2×10^5 PC12 cells were transfected with 250 ng of pc3.1-mCysLT$_2$ or vector alone, 300 ng of zif268-firefly luciferase/pGL2, and 250 ng of thymidine kinase-*Renilla* luciferase/pRL (Promega) and seeded in collagen-coated 24-well plates. After serum starvation for 1.5 h, they were stimulated with ligands for 6 h. Firefly

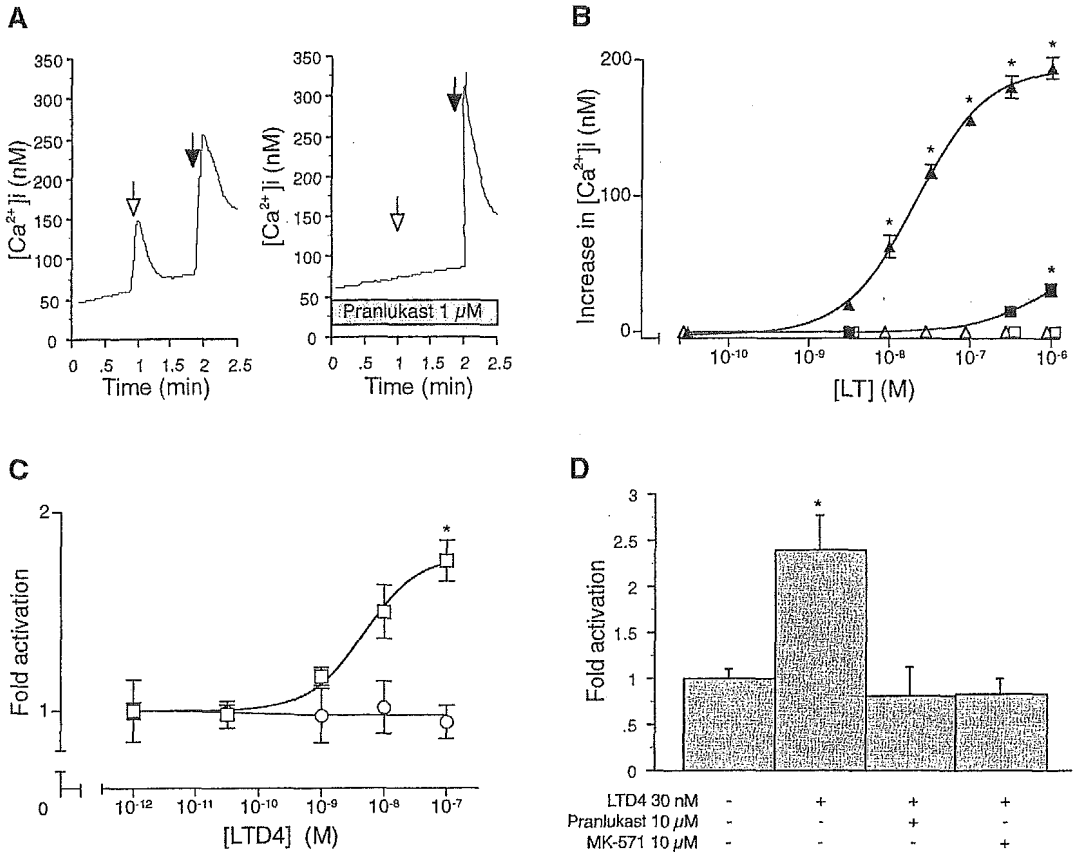

FIG. 2. **Ca^{2+} response and reporter gene expression using $mCysLT_1$.** *A* and *B*, Ca^{2+} mobilization in HEK-293 cells stably expressing $mCysLT_1$. *A*, the $mCysLT_1$-expressing cells (HEK 7-1) loaded with Fura2-AM were challenged with 100 nM LTD_4 (*open arrow*) or 10 μM ATP (*closed arrow*), and the change in $[Ca^{2+}]_i$ was measured. The *right panel* shows the response of the cells treated with 10 μM pranlukast 5 min before the challenge. The results are representatives of three independent experiments. *B*, HEK 7-1 cells were loaded with Fura2-AM and stimulated with various concentrations of LTC_4 (■) or LTD_4 (▲). Vector-transfected HEK-293 cells stimulated with LTC_4 (□) or LTD_4 (Δ) were used as negative controls. The differences of $[Ca^{2+}]_i$ before and after the challenges are shown ($n = 3$, means ± S.E.). Statistically significant differences between the vector control and HEK 7-1 are indicated. *, $p < 0.01$, unpaired *t* test. *C* and *D*, reporter gene assays of B103 cells transiently transfected with $mCysLT_1$ or vector alone. *C*, Cells transfected with $mCysLT_1$ (□) or vector alone (○) were stimulated with various concentrations of LTD_4. The data are expressed as fold activation over control (without LTD_4) and expressed as the means ± S.E. ($n = 3$). Statistically significant differences between the control and the LT-stimulated cells are indicated. *, $p < 0.05$, unpaired *t* test. *D*, the effects of two $CysLT_1$ antagonists are shown. The data are expressed as fold activation over the control (without LTD_4) and expressed as the means ± S.E. ($n = 4$). Statistically significant differences between the control and the drug-treated cells are indicated. *, $p < 0.05$, Bonferroni's multiple *t* test.

and *Renilla* luciferase activities were measured using PICAGENE Dual Seapansy and a Mini Lumat LB9506 luminometer (Berthold, Bad Wildbad, Germany). Firefly luciferase values were standardized to *Renilla* values.

Northern Blotting—Total RNA was extracted from 129+Ter/Sv Jcl (Clea Japan, Tokyo, Japan) and C57BL/6J Jcl (Clea Japan) mouse tissues including brain, heart, lung, liver, spleen, kidney, small intestine, skeletal muscle, and skin, using Isogen (Wako, Osaka, Japan). Poly(A)$^+$ RNA was isolated from 200 μg of the total RNA using a μMACS mRNA isolation kit (Miltenyi Biotec, Bergisch Gladbach, Germany). The RNA samples were denatured, electrophoresed on 0.7% formaldehyde-agarose gels, and transferred onto nylon membranes Hybond-N+ (Amersham Biosciences) as described (26). The membranes were hybridized with [α-^{32}P]dCTP-labeled ORF of $mCysLT_1$, $mCysLT_2$, or human glyceraldehyde-3-phosphate dehydrogenase (G3PDH) at 65 °C for 2 h in a Rapid Hyb hybridization solution (Amersham Biosciences). The membranes were washed at 65 °C in 0.2× SSC, 0.1% SDS for 1 h and subjected to autoradiography for 5 days ($mCysLT_1$ and $mCysLT_2$) or overnight (G3PDH).

Quantitative Real Time Reverse Transcriptase-PCR—Total RNA was prepared as described above from 129 and C57BL/6 mouse adrenal gland, peritoneal macrophages, and spleen. For elicitation of peritoneal macrophages, the animals were injected with 2 ml of 4% thioglycollate broth 4 days prior to sacrifice and peritoneal lavage using ice-cold PBS with 2 mM EDTA. cDNA was synthesized from 1 μg of total RNA using Superscript II (Invitrogen) and 50 ng of random hexamers according to the manufacturer's protocol, and 2 μl of the cDNA was diluted in 38 μl of 10 mM Tris-HCl, 1 mM EDTA (pH 8.0) for PCR. PCR was carried out using a LightCycler System (Roche Molecular Biochemicals), and the products were detected by measuring the binding of the fluorescence dye SYBR Green I to double-stranded DNA. The PCR reactions were set up in microcapillary tubes in a volume of 20 μl. The reaction components were 1 μl of diluted cDNA, 1 × FastStart DNA Master SYBR Green I (Roche Molecular Biochemicals), a final concentration of 3 mM $MgCl_2$, and 1 μM upstream and downstream primers. pc4HM-$mCysLT_1$, pc3.1-$mCysLT_2$, and an expressed sequence tag clone containing mG3PDH cDNA (GenBank™ accession number BF537941) purchased from IncyteGenomics (Palo Alto, CA) were used as standards. Primers were chosen so that they would yield PCR products identical in DNA sequence from 129 and C57BL/6 inbred strains. The following primers were used: mCys1-760+, 5′-CAACGAACTATCCACCTTCACC-3′; mCys1-923−, 5′-AGCCTTCTCCTAAAGTTTCCAC-3′; mCys2-662+, 5′-GTCCACGTGCTGCTCATAGG-3′; mCys2-843−, 5′-ATTGGCTGCAGCCATGGTC-3′; mG3PDH-879+, 5′-AGGTTGTCTCCTGCGACTTC-3′; and mG3PDH-1089−, 5′-CTTGCTCAGTGTCCTTGCTG-3′. These primer pairs result in PCR products of 164 ($mCysLT_1$), 182 ($mCysLT_2$), and 211 bp (G3PDH). The standards and the samples were simultaneously amplified using the same reaction master mixture. The reactions were incubated at 95 °C for 10 min to activate the polymerase, followed by 50 cycles of amplification. Each cycle of PCR included 3 s of denaturation at 95 °C, 3 s of primer annealing at 67 °C for G3PDH, 65 °C for $mCysLT_1$, and 68 °C for $mCysLT_2$, and 10 s of extension at 72 °C. The temperature ramp was 20 °C/s. At the end of the extension steps, the fluorescence of each sample was measured to allow quantification of the cDNAs. After cycling, melting curves of the PCR products were acquired by stepwise increase of the temperature from 5 °C above the annealing temperature to 95 °C. Using LightCycler analysis software, the SYBR Green I signal of each sample was plotted *versus* the

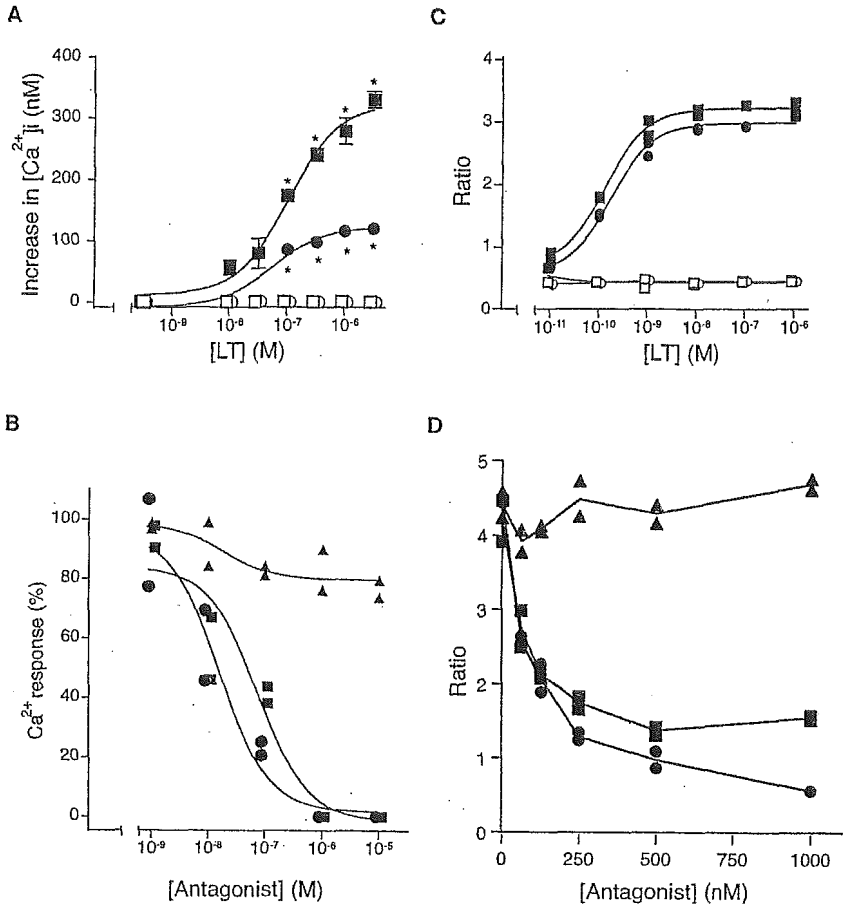

FIG. 3. **Ca^{2+} response and reporter gene expression using $mCysLT_2$.** *A* and *B*, Ca^{2+} mobilization in CHO cells stably expressing $mCysLT_2$. The cells were loaded with Fura2-AM and challenged with LTC_4 or LTD_4. The increase in $[Ca^{2+}]_i$ was calculated from the fluorescence ratio (340 nm/380 nm). *A*, $[Ca^{2+}]_i$ increases of $mCysLT_2$-expressing cells (CHO-7A1) challenged with LTC_4 (■) or LTD_4 (●) and vector control cells challenged with LTC_4 (□) or LTD_4 (○) are shown ($n = 3$, means ± S.E.). Statistically significant differences between the control and CHO-7A1 are indicated. *, $p < 0.01$, unpaired *t* test. *B*, effects of CysLT antagonists were examined. The increase in $[Ca^{2+}]_i$ after 100 nM LTC_4 stimulation is shown as a percentage to that of the cells without an antagonist ($n = 2$, each replicate shown). BAY u9773 (■) and pranlukast (●) inhibited the response to LTC_4, whereas MK-571 (▲) did not affect the response to the LTC_4 stimulation. Neither MK-571, pranlukast, nor BAY u9773 affected Ca^{2+} response to 10 μM ATP ($n = 2$, data not shown). *C* and *D*, reporter gene assay of PC12 cells transiently transfected with $mCysLT_2$ or vector alone. The ratios of firefly luciferase activity to *Renilla* luciferase activity are shown. *C*, the responses of $mCysLT_2$-transfected cells challenged with various concentrations of LTC_4 (■) or LTD_4 (●) and vector-transfected cells challenged with LTC_4 (□) or LTD_4 (○) are shown ($n = 2$, each replicate shown). The experiments using LTC_4 were performed in the presence of 5 mM serine and 10 mM borate. *D*, the responses to 10 nM LTD_4 in the presence of various concentrations of MK-571 (▲), pranlukast (●), or BAY u9773 (■) are shown ($n = 2$, each replicate shown).

number of cycles, and the crossing points were obtained. These crossing points correlate inversely with the log of the initial template concentration. The levels of mRNA were estimated by subtracting the initial levels of target DNA in PCR reactions without reverse transcription, which represents genomic contamination. Then the mRNA levels were normalized to the level of G3PDH mRNA.

In Situ Hybridization—Paraffin sections of the skin samples from 129 and C57BL/6 mice fixed in 10% formalin were investigated as described previously (27, 28) by using a slightly modified nonradioactive *in situ* hybridization technique with digoxigenin-labeled RNA probes. Briefly, paraffin-embedded tissues were cut to 4-μm-thin sections, mounted onto silane-coated slides, deparaffinized, and treated with proteinase K (5 μg/ml in PBS) for 10 min at 24 °C and glycine (2 mg/ml in PBS) for 15 min at 24 °C. Then the sections were acetylated with acetic anhydride (1 ml in 400 ml of 0.1 M triethanolamine, pH 8.0) for 15 min at 24 °C. After washing with PBS, the samples were soaked in 2× SSC with 50% formamide, subjected to hybridization. Fragments of cDNAs for mCysLTs ($mCysLT_1$ ORF at 687–887 and $mCysLT_2$ ORF at 18–222) were amplified by PCR using upstream primers with a recognition sequence for *Hin*dIII and downstream primers with a recognition sequence for *Eco*RI, and subcloned into pSPT18 by directional cloning. The plasmids were linearized using *Hin*dIII to prepare the antisense probes and *Eco*RI for the sense probes. The probes were labeled with digoxigenin-11-UTP using a DIG RNA labeling kit (Roche Molecular Biochemicals). The labeled RNA probes (1 μg/ml) in a mixture containing 50% formamide, 10% dextran sulfate, 2× SSC, 1 mg/ml tRNA, 1 mg/ml salmon sperm DNA, and 0.1% bovine serum albumin were placed on the slides and coverslipped. Hybridization was performed in a humidified chamber for 16 h at 42 °C for the $mCysLT_1$ probe and 50 °C for the $mCysLT_2$ probe. The slides were washed in 2× SSC with 50% formamide for 20 min three times at 42 °C. Nonhybridized probes were digested in 20 μg/ml RNase A, 500 mM NaCl, 1 mM EDTA, and 10 mM Tris-HCl (pH 8.0) for 30 min at 37 °C. They were then rinsed for 20 min in 0.1× SSC three times at 42 °C. The digoxigenin-labeled probes were visualized using a DIG nucleic acid detection kit (Roche Molecular Biochemicals) according to the manufacturer's protocol. The slides were counterstained in methyl green for 10 min, washed in running tap water, and mounted.

RESULTS AND DISCUSSION

The Structure of $mCysLT_1$ and $mCysLT_2$—$mCysLT_1$ and $mCysLT_2$ were predicted to be polypeptides of 339 and 309 amino acid residues, respectively (Fig. 1*A*). The identities of the amino acid sequences between 129 mouse and human (16–18) CysLTs are shown in Fig. 1*B*. $mCysLT_1$ was longer than human $CysLT_1$ by two amino acid residues. $mCysLT_2$ was shorter than human $CysLT_2$ by 37 amino acid residues, being truncated at both the N and C termini. The sequence of $mCysLT_1$ was identical among 129, C57BL/6, and BALB/c mice, and there was a mismatch in $mCysLT_2$ sequences at the 213th amino acid residue between 129 (Val) and C57BL/6 (Ile). The preserved amino acids in the rhodopsin-like G protein-coupled

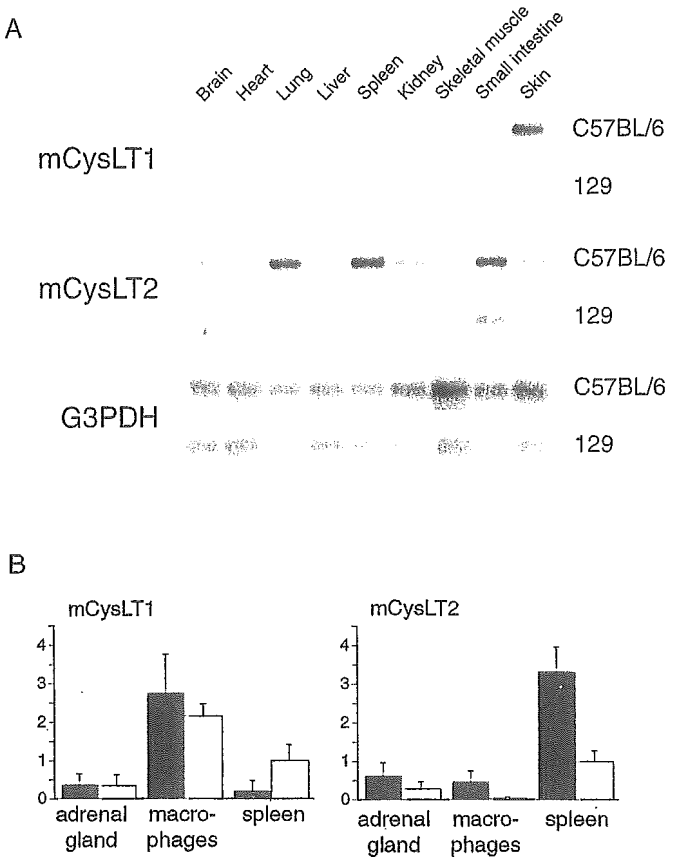

FIG. 4. **Expression of mCysLT$_1$ and mCysLT$_2$ mRNA in various tissues of C57BL/6 and 129 inbred strains.** *A*, Northern blot analysis. Poly(A)$^+$ RNAs (3 μg) were electrophoretically separated, transferred to nylon membranes, and hybridized with [α-^{32}P]dCTP-labeled ORFs of mCysLT$_1$, mCysLT$_2$, and human G3PDH. The shown data are representative of three experiments that gave similar results. *B*, quantitative real time reverse transcriptase-PCR. mRNA levels of C57BL/6 mice (*closed bar*) and 129 mice (*open bar*) were obtained as described under "Materials and Methods" and given as fold expression compared with the levels of 129 spleen (n = 3, means ± S.E.). The differences in expression levels between strains were seen in CysLT$_2$ of the spleen ($p < 0.05$).

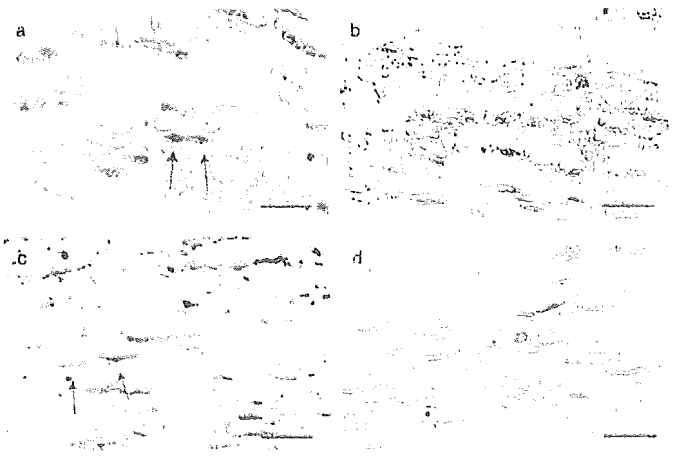

FIG. 5. ***In situ* hybridization of CysLT$_1$ and CysLT$_2$ mRNA in 129 mouse skin.** *a* and *b*, *in situ* hybridization of CysLT$_1$. *a*, antisense probe, showing expression in subcutaneous fibroblasts (*arrows*). *b*, sense control probe. *c* and *d*, *in situ* hybridization of CysLT$_2$. *c*, antisense probe, showing expression in subcutaneous fibroblasts (*arrows*). *d*, sense control probe. *Scale bars* are 50 μm.

receptor family, including two Cys residues in the first and second extracellular loops, Asp in transmembrane domain 2 (TM2), Trp in TM4, Tyr in TM5, and Pro in TM6, were all present in mCysLT$_1$ and mCysLT$_2$. mCysLT$_2$ had the Asn-Pro-Xaa$_2$-Tyr motif at the end of the TM7, whereas mCysLT$_1$ had an Asp residue instead of Asn in the motif. There was no Asp-Arg-Tyr motif at the TM3/intracellular loop 2 transition in mCysLT$_1$ nor mCysLT$_2$, although it is a highly conserved motif in the G protein-coupled receptor family. Both mCysLT$_1$ and mCysLT$_2$ had possible phosphorylation sites in intracellular loop 3 and the C terminus, and CysLT$_1$ had several possible *N*-glycosylation sites in the N terminus and extracellular loops.

Pharmacological Properties of mCysLT$_1$ and mCysLT$_2$—Mouse orthologues of CysLT$_1$ and CysLT$_2$ were identified as functional cysteinyl LT receptors by several methods. CysLT$_1$ and CysLT$_2$ are known to increase $[Ca^{2+}]_i$ (20, 29). LTD$_4$ evoked a dose-dependent increase in $[Ca^{2+}]_i$ in HEK-293 cell lines stably expressing mCysLT$_1$ (HEK 7-1 (Fig. 2, *A* and *B*) and HEK 7-3 (data not shown)). LTC$_4$ also evoked a slight increase in $[Ca^{2+}]_i$ (Fig. 2*B*), whereas LTB$_4$ or LTE$_4$ did not (data not shown). These cells pretreated with a CysLT$_1$ antagonist, pranlukast (Fig. 2*A*) or MK-571 (data not shown), did not respond to LTD$_4$, whereas they remained responsive to ATP. In a reporter gene assay, B103 cells transiently expressing mCysLT$_1$ increased luciferase activity in response to LTD$_4$ in a dose-dependent manner (Fig. 2*C*). The cells did not respond to either LTB$_4$ or LTE$_4$ at a concentration of 10 or 100 nM (data not shown). The LTD$_4$-induced response was inhibited by pranlukast or MK-571 (Fig. 2*D*).

In CHO cells stably expressing mCysLT$_2$ (CHO-7A1), LTC$_4$ and LTD$_4$ exhibited dose-dependent increases in $[Ca^{2+}]_i$ (Fig. 3*A*). The response was inhibited by BAY u9773, a nonselective antagonist of cysteinyl LT receptors (30), in a dose-dependent manner but was not inhibited by a CysLT$_1$-specific antagonist, MK-571 (Fig. 3*B*). The response of CHO-8B3 cells, another mCysLT$_2$-expressing clone, was similar to that of CHO-7A1 (n = 3; data not shown). ATP (10 μM) elicited the same level of increase in $[Ca^{2+}]_i$ in CHO-7A1, CHO-8B3, and the vector control (n = 3; data not shown). PC12 cells transiently expressing mCysLT$_2$ increased luciferase activities in response to LTC$_4$ and LTD$_4$ to the same extent in dose-dependent manners (Fig. 3*C*), and the responses were inhibited by BAY u9773 and not by MK-571 (Fig. 3*D*). Surprisingly, pranlukast, found to be a CysLT$_1$-specific antagonist from human studies (16, 17), inhibited the LTC$_4$-induced increase in $[Ca^{2+}]_i$ (Fig. 3*B*) and the LTD$_4$-induced luciferase activity (Fig. 3*D*) in the cells expressing mCysLT$_2$. Several reports showing that pranlukast does not antagonize human CysLT$_2$ (18, 20) imply a pharmacological difference of CysLT$_2$ between human and mouse likely because of significant difference in primary structure (Fig. 1*B*). BAY u9773 was partially agonistic on mCysLT$_2$ as is reported in human CysLT$_2$ (19) (data not shown).

Different Tissue Distribution of CysLT$_1$ and CysLT$_2$ mRNA in Two Mouse Inbred Strains—Hybridization of poly(A)$^+$ RNA from various mouse tissues detected transcripts of 3.0 and 5.5 kb for CysLT$_1$ and CysLT$_2$, respectively (Fig. 4*A*). As a whole, the expression levels of CysLTs were higher in C57BL/6 inbred strain than in 129 inbred strain, even though a slight difference in control hybridization (G3PDH) in Northern blotting was observed in some tissues. In C57BL/6 strain, the highest mRNA expression for CysLT$_1$ was observed in skin, lung, small intestine, and macrophages, and moderate expressions were found in other tissues; the expression of CysLT$_2$ was ubiquitous with higher expressions in spleen, lung, and small intestine (Fig. 4). Differential tissue expression between two strains suggests that regulatory polymorphism is present.

Given the importance of cysteinyl LTs in skin diseases including atopic dermatitis (31), we investigated the distribution of CysLTs in mouse skin by *in situ* hybridization. We chose 129 inbred strain because Goulet *et al.* (32) had reported the potent inflammatory response of the skin in 129 mice. No signals of

CysLTs were detected in epidermis (data not shown). In the subcutaneous connective tissues, however, high expressions of $CysLT_1$ (Fig. 5*a*) and $CysLT_2$ mRNA (Fig. 5*c*) were seen mostly in fibroblasts. No signal was obtained using the sense control (Fig. 5, *b* and *d*). It has been reported that cysteinyl LTs increase collagen synthesis in fibroblasts (33, 34), and our report is the first to demonstrate the expression of CysLTs in fibroblasts. Further study is needed to uncover yet unknown roles of cysteinyl LTs in wound healing and pathological collagen synthesis.

In conclusion, we have cloned $mCysLT_1$ and $mCysLT_2$ and found differences in the pharmacological characteristics between mouse and human $CysLT_2$. There are differences in mRNA expression of $CysLT_1$ and $CysLT_2$ between mouse strains, suggesting the importance of choosing a proper mouse strain for a disease model. We also discovered expression of both CysLTs in subcutaneous fibroblasts. These data are useful in interpreting and understanding the physiological and pathological roles of CysLTs in animal models of human diseases.

Acknowledgments—We thank Drs. D. A. Wong, S. Sato, and K. Kishimoto for suggestions and M. Ito for technical assistance.

REFERENCES

1. Murphy, R. C., Hammarstrom, S., and Samuelsson, B. (1979) *Proc. Natl. Acad. Sci. U. S. A.* **76,** 4275–4279
2. Shimizu, T., and Wolfe, L. S. (1990) *J. Neurochem.* **55,** 1–15
3. Samuelsson, B. (1983) *Science* **220,** 568–575
4. Samuelsson, B., Dahlen, S. E., Lindgren, J. A., Rouzer, C. A., and Serhan, C. N. (1987) *Science* **237,** 1171–1176
5. Welsch, D. J., Creely, D. P., Hauser, S. D., Mathis, K. J., Krivi, G. G., and Isakson, P. C. (1994) *Proc. Natl. Acad. Sci. U. S. A.* **91,** 9745–9749
6. Lam, B. K. (1997) *Front. Biosci.* **2,** 380–386
7. Penrose, J. F., and Austen, K. F. (1999) *Proc. Assoc. Am. Physicians* **111,** 537–546
8. Dahlen, S. E., Hedqvist, P., Hammarstrom, S., and Samuelsson, B. (1980) *Nature* **288,** 484–486
9. Piper, P. J. (1984) *Physiol. Rev.* **64,** 744–761
10. Lewis, R. A., Austen, K. F., and Soberman, R. J. (1990) *N. Engl. J. Med.* **323,** 645–655
11. Drazen, J. M. (1998) *Am. J. Respir. Crit. Care Med.* **158,** (suppl.) 193–200
12. Jones, T. R., Labelle, M., Belley, M., Champion, E., Charette, L., Evans, J., Ford-Hutchinson, A. W., Gauthier, J. Y., Lord, A., Masson, P., McAuliffe, M., McFarlane, C. S., Metters, K. M., Pickett, C., Piechuta, H., Rochette, C., Rodger, I. W., Sawyer, N., Young, R. N., Zamboni, R., and Abraham, W. M. (1995) *Can. J. Physiol. Pharmacol.* **73,** 191–201
13. Reiss, T. F., Chervinsky, P., Dockhorn, R. J., Shingo, S., Seidenberg, B., and Edwards, T. B. (1998) *Arch. Intern. Med.* **158,** 1213–1220
14. Suissa, S., Dennis, R., Ernst, P., Sheehy, O., and Wood-Dauphinee, S. (1997) *Ann. Intern. Med.* **126,** 177–183
15. Obata, T., Okada, Y., Motoishi, M., Nakagawa, N., Terawaki, T., and Aishita, H. (1992) *Jpn. J. Pharmacol.* **60,** 227–237
16. Lynch, K. R., O'Neill, G. P., Liu, Q., Im, D. S., Sawyer, N., Metters, K. M., Coulombe, N., Abramovitz, M., Figueroa, D. J., Zeng, Z., Connolly, B. M., Bai, C., Austin, C. P., Chateauneuf, A., Stocco, R., Greig, G. M., Kargman, S., Hooks, S. B., Hosfield, E., Williams, D. L., Jr., Ford-Hutchinson, A. W., Caskey, C. T., and Evans, J. F. (1999) *Nature* **399,** 789–793
17. Sarau, H. M., Ames, R. S., Chambers, J., Ellis, C., Elshourbagy, N., Foley, J. J., Schmidt, D. B., Muccitelli, R. M., Jenkins, O., Murdock, P. R., Herrity, N. C., Halsey, W., Sathe, G., Muir, A. I., Nuthulaganti, P., Dytko, G. M., Buckley, P. T., Wilson, S., Bergsma, D. J., and Hay, D. W. (1999) *Mol. Pharmacol.* **56,** 657–663
18. Heise, C. E., O'Dowd, B. F., Figueroa, D. J., Sawyer, N., Nguyen, T., Im, D. S., Stocco, R., Bellefeuille, J. N., Abramovitz, M., Cheng, R., Williams, D. L., Jr., Zeng, Z., Liu, Q., Ma, L., Clements, M. K., Coulombe, N., Liu, Y., Austin, C. P., George, S. R., O'Neill, G. P., Metters, K. M., Lynch, K. R., and Evans, J. F. (2000) *J. Biol. Chem.* **275,** 30531–30536
19. Nothacker, H. P., Wang, Z., Zhu, Y., Reinscheid, R. K., Lin, S. H., and Civelli, O. (2000) *Mol. Pharmacol.* **58,** 1601–1608
20. Takasaki, J., Kamohara, M., Matsumoto, M., Saito, T., Sugimoto, T., Ohishi, T., Ishii, H., Ota, T., Nishikawa, T., Kawai, Y., Masuho, Y., Isogai, T., Suzuki, Y., Sugano, S., and Furuichi, K. (2000) *Biochem. Biophys. Res. Commun.* **274,** 316–322
21. Maekawa, A., Kanaoka, Y., Lam, B. K., and Austen, K. F. (2001) *Proc. Natl. Acad. Sci. U. S. A.* **98,** 2256–2261
22. Henderson, W. R., Jr., Lewis, D. B., Albert, R. K., Zhang, Y., Lamm, W. J., Chiang, G. K., Jones, F., Eriksen, P., Tien, Y. T., Jonas, M., and Chi, E. Y. (1996) *J. Exp. Med.* **184,** 1483–1494
23. Jones, T. R., Zamboni, R., Belley, M., Champion, E., Charette, L., Ford-Hutchinson, A. W., Frenette, R., Gauthier, J. Y., Leger, S., Masson, P., McFarlane, C. S., Piechuta, H., Rokach, J., Williams, H., and Young, R. N. (1989) *Can. J. Physiol. Pharmacol.* **67,** 17–28
24. Yamazawa, T., Iino, M., and Endo, M. (1992) *FEBS Lett.* **301,** 181–184
25. Kawasawa, Y., Kume, K., Izumi, T., and Shimizu, T. (2000) *Biochem. Biophys. Res. Commun.* **276,** 957–964
26. Chomczynski, P. (1992) *Anal. Biochem.* **201,** 134–139
27. Igarashi, A., Nashiro, K., Kikuchi, K., Sato, S., Ihn, H., Fujimoto, M., Grotendorst, G. R., and Takehara, K. (1996) *J. Invest. Dermatol.* **106,** 729–733
28. Igarashi, A., Nashiro, K., Kikuchi, K., Sato, S., Ihn, H., Grotendorst, G. R., and Takehara, K. (1995) *J. Invest. Dermatol.* **105,** 280–284
29. Chan, C. C., Ecclestone, P., Nicholson, D. W., Metters, K. M., Pon, D. J., and Rodger, I. W. (1994) *J. Pharmacol. Exp. Ther.* **269,** 891–896
30. Coleman, R. A., Eglen, R. M., Jones, R. L., Narumiya, S., Shimizu, T., Smith, W. L., Dahlen, S. E., Drazen, J. M., Gardiner, P. J., Jackson, W. T., Jones, T. R., Krell, R. D., and Nicosia, S. (1995) *Adv. Prostaglandin. Thromboxane. Leukot. Res.* **23,** 283–285
31. Hishinuma, T., Suzuki, N., Aiba, S., Tagami, H., and Mizugaki, M. (2001) *Br. J. Dermatol.* **144,** 19–23
32. Goulet, J. L., Byrum, R. S., Key, M. L., Nguyen, M., Wagoner, V. A., and Koller, B. H. (2000) *J. Immunol.* **164,** 4899–4907
33. Phan, S. H., McGarry, B. M., Loeffler, K. M., and Kunkel, S. L. (1988) *Biochemistry* **27,** 2846–2853
34. Abe, M., Kurosawa, M., Ishikawa, O., and Miyachi, Y. (2000) *J. Allergy Clin. Immunol.* **106,** (suppl.) 78–84

British Journal of Pharmacology (2002) 135, 1213–1218 © 2002 Nature Publishing Group All rights reserved 0007–1188/02 $25.00
www.nature.com/bjp

Platelet-activating factor drives eotaxin production in an allergic pleurisy in mice

[1]André Klein, [1]Vanessa Pinho, [1]Ana Letícia Alessandrini, [2]Takao Shimizu, [2]Satoshi Ishii & *,[1]Mauro M. Teixeira

[1]Immunopharmacology, Departamento de Bioquímica e Imunologia, ICB, Universidade Federal de Minas Gerais, Belo Horizonte, Brazil and [2]Department of Biochemistry and Molecular Biology, Faculty of Medicine, The University of Tokyo, Japan

1 The activation of eosinophils *via* G-protein-coupled seven transmembran receptors play a necessary role in the recruitment of these cells into tissue. The present study investigates a role for PAF in driving eotaxin production and eosinophil recruitment in an allergic pleurisy model in mice.

2 The intrapleural injection of increasing doses of PAF (10^{-11} to 10^{-9} moles per cavity) induced a dose- and PAF receptor-dependent recruitment of eosinophils 48 h after stimulation.

3 Intrapleural injection of PAF induced the rapid (within 1 h) release of eotaxin into the pleural cavity of mice and an anti-eotaxin antibody effectively inhibited PAF-induced recruitment of eosinophils.

4 Eosinophil recruitment in the allergic pleurisy was markedly inhibited by the PAF receptor antagonist UK-74,505 (modipafant, 1 mg kg^{-1}). Moreover, recruitment of eosinophils in sensitized and challenged PAF receptor-deficient animals was lower than that observed in wild-type animals.

5 Blockade of PAF receptors with UK-74,505 suppressed by 85% the release of eotaxin in the allergic pleurisy.

6 Finally, the injection of a sub-threshold dose of PAF and eotaxin cooperated to induce eosinophil recruitment *in vivo*.

7 In conclusion, the production of PAF in an allergic reaction could function in multiple ways to facilitate the recruitment of eosinophils – by facilitating eotaxin release and by cooperating with eotaxin to induce greater recruitment of eosinophils.

British Journal of Pharmacology (2002) **135**, 1213–1218

Keywords: Eosinophils; eotaxin; platelet-activating factor; recruitment; chemokines

Abbreviations: LTB_4, Leukotriene B_4; OVA, ovalbumin; PAF, platelet-activating factor; $PAFR^{-/-}$, PAF receptor-deficient; PBS, phosphate-buffered saline; SCF, stem cell factor

Introduction

Eosinophils are typically tissue-dwelling cells and appear to play an important role in the pathogenesis of allergic diseases, such as asthma and atopic dermatitis (Cara *et al.*, 1999). There has been much interest in the understanding of the mechanisms underlying eosinophil recruitment *in vivo* as this knowledge may aid in the development of novel strategies for the treatment of allergic disorders (Teixeira *et al.*, 1995; Giembycz & Lindsay, 1999). The activation of eosinophils *via* G-protein-coupled seven transmembrane receptors play a necessary role in the recruitment of these cells into tissue and may, thus, be good targets for drug development (Teixeira *et al.*, 1995; 1997a,b).

We have recently shown that the cytokine stem cell factor (SCF) played an important role for the migration of eosinophils in an allergic pleurisy model in mice (Klein *et al.*, 2000). Of interest, SCF appeared to drive the local production of LTB_4 which cooperated with eotaxin to induce eosinophil recruitment (Klein *et al.*, 2001). Whereas SCF induced significant eotaxin production, the blockade of SCF did not inhibit the release of eotaxin following allergen challenge of sensitized animals (Klein *et al.*, 2001). Thus, it was not clear from our studies the mediator(s) underlying local eotaxin production and release.

Several studies have demonstrated the ability of the lipid mediator platelet-activating factor (PAF) to induce eosinophil recruitment and activation *in vivo* and *in vitro* (e.g. Silva *et al.*, 1991; Teixeira *et al.*, 1994; 1997a; Alves *et al.*, 1996). Indeed, PAF induces chemoattraction, activation of several other functions and priming of eosinophils and other cell types (e.g. van der bruggen *et al.*, 1994; Schweizer *et al.*, 1996; Ishii & Shimizu, 2000). Moreover, endogenous production of PAF may be involved in the effector function of eosinophils (e.g.: Tool *et al.*, 1992; Bartemes *et al.*, 1999) and in the modulation of the production of chemokines (e.g.: Maruoka *et al.*, 2000; Au *et al.*, 2001) in response to several stimuli. Here, using a PAF receptor antagonist (UK-74,505) and PAF receptor-deficient animals ($PAFR^{-/-}$), we investigated whether PAF participated in the cascade of events leading to mediator release and eosinophil recruitment in our allergic pleurisy model.

*Author for correspondence at: Departamento de Bioquímica e Imunologia, Instituto de Ciências Biológicas, Universidade Federal de Minas Gerais, Av. Antonio Carlos, 6627-Pampulha, 31270-901 Belo Horizonte MG Brazil; E-mail: mmtex@mono.icb.ufmg.br

Methods

Animals

Male BALB/C mice (18–22 g) were used throughout these experiments. Animals were housed in a temperature-controlled room with free access to water and food. All experimental procedures have been subjected to evaluation and were approved by the local Animal Ethics Committee. PAF receptor deficient animals were generated as previously described (Ishii *et al.*, 1998) and intercrossed for at least seven generations to establish the BALB/c strain.

Drugs and reagents

Recombinant murine eotaxin was purchased from Peprotech (London, U.K.). Eotaxin was dissolved in water, diluted further in phosphate buffered saline (PBS, pH 7.4) containing 0.01% bovine serum albumin and stored at −20°C until use. Bovine serum albumin, ovalbumin (OVA) and control rabbit serum were purchased from Sigma. PAF was purchased from Calbiochem. The specific and long-acting PAF receptor antagonist UK-74,505 (Modipafant, 4-(chlorophenyl)-1,4-dihydro-3-ethoxycarbonyl-6-methyl-2-[4-(2-methylimidazol[4,5-c]phenyl-5-[N-(2-pyridyl)carbomoyl]pyridine) (Alabaster *et al.*, 1991; Jezequel *et al.*, 1996) was a gift from Pfizer Global Research and Development, Kent, U.K. UK-74,505 was dissolved in HCl 0.01 N and further diluted in PBS. Control animals received drug vehicle.

Sensitization

Animals were immunized with OVA adsorbed to aluminium hydroxide gel as previously described (Das *et al.*, 1997). Briefly, mice were injected s.c. on days 1 and 8 with 0.2 ml of a solution containing 100 μg of OVA and 70 μg of aluminium hydroxide (Reheiss, Dublin, Ireland).

Leukocyte migration into the pleural cavity induced by PAF or antigen

PAF (10^{-11} to 10^{-9} mol per cavity) was injected intrapleurally (i.pl.) in naïve mice, and animals killed at 48 h after the i.pl. injection. In some experiments, low doses of eotaxin and PAF were mixed prior to their i.pl. injection. Sensitized mice were challenged with antigen (OVA) or PBS. The cells present in the pleural cavity were harvested by injecting 2 ml of PBS and total cell counts performed in a modified Neubauer chamber using Turk's stain. Differential cell counts were performed on cytospin preparations (Shandon III) stained with May-Grumwald-Giemsa using standard morphologic criteria to identify cell types. The results are presented as the number of cells per cavity.

PAF receptor antagonist or anti-eotaxin pretreatment

In order to investigate the role of endogenous PAF on the eosinophil recruitment induced by PAF or ovalbumin in immunized animals, the PAF receptor antagonist UK-74,505 (0.1 to 1.0 mg kg^{-1}) was administered i.p. 60 min prior to the stimulus, and the number of infiltrating eosinophils was assessed 48 hours after. This dose range has been shown to be effective at blocking PAF receptors in rodents (Miotla *et al.*, 1998; Borges *et al.*, 2000). A rabbit polyclonal anti-eotaxin antibody was prepared and purified over protein A column as previously described (Ruth *et al.*, 1998). This antibody is specific for eotaxin and not shown to cross-react to other known murine chemokines (Ruth *et al.*, 1998). Anti-eotaxin was administered i.p. at the dose of 100 μg per mouse 60 min prior to the i.pl. administration of PAF. In some experiments, the eosinophil recruitment 48 h after antigen challenge in $PAFR^{-/-}$ mice was compared to that of age- and sex-matched wild-type animals.

Measurement of eotaxin

Frozen supernatants obtained from pleural cavity washes at different times (1–24 h) after challenge with PAF (10^{-9} moles per cavity) were used for eotaxin detection. The effects of the PAF receptor antagonist was assessed by injecting UK-74,505 (1 mg kg^{-1}, i.p.) 60 min prior to antigen challenge. Six hours later, the pleural cavity was washed and the levels of eotaxin assessed on the supernatant.

The concentration of eotaxin protein in pleural effluents was measured by specific ELISA using commercially available antibody pairs and as specified by the supplier (R&D Systems, Minneapolis, MN, USA).

Statistical analysis

All results are presented as the mean ± s.e.mean. Normalized data were analysed by one-way ANOVA, and differences between groups were assessed using the Student-Newman-Keuls post-test. A P value <0.05 was considered significant.

Results

PAF induces eosinophil recruitment and eotaxin production in the pleural cavity of mice

The intrapleural injection of increasing doses of PAF (10^{-11} to 10^{-9} moles per cavity) induced a dose-dependent recruitment of eosinophils 48 h after stimulation (Figure 1). At this time point, a significant recruitment of mononuclear cells, but not neutrophils, was also observed (data not shown). These effects of PAF were PAF receptor-dependent as demonstrated by the ability of the PAF receptor antagonist UK-74,505 to abrogate PAF-induced eosinophil recruitment (PBS, 0.2 ± 0.1 eosinophils × 10^5 per cavity; PAF 10^{-9} moles, 1.4 ± 0.3; PAF + UK-74,505 0.1 mg kg^{-1}; 0.4 ± 0.1; PAF + UK-74,505 1.0 mg kg^{-1}, 0.2 ± 0.1; $n=5$ in each group, $P<0.01$).

Next, we examined whether PAF could induce the release of eotaxin into the pleural cavity of mice. As seen in Figure 2A, significant levels of eotaxin were detected as early as 1 h after the injection of PAF in the pleural cavity of naïve mice. Elevated concentrations of eotaxin were also detected at 3 h and levels had dropped to background 6 h after PAF injection (Figure 2A). Not only was eotaxin induced after injection of PAF, but, more importantly, an anti-eotaxin antibody effectively inhibited the recruitment of eosinophils observed after injection of PAF (Figure 2B).

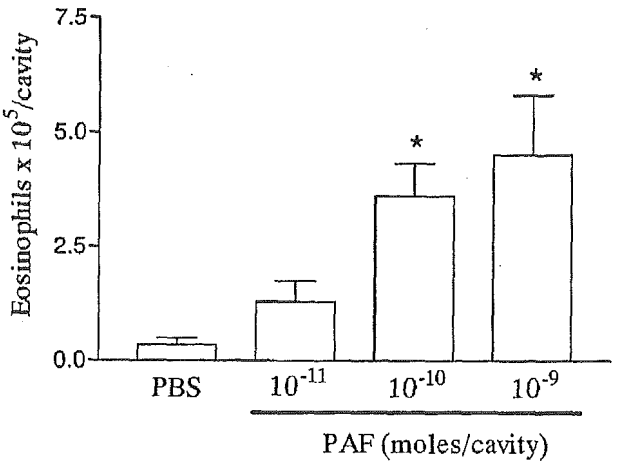

Figure 1 Dose-dependent effects of PAF on the recruitment of eosinophils to the pleural cavity of mice. In dose-response experiments, phosphate-buffered saline (PBS, 100 μl) or PAF (10^{-11} to 10^{-9} moles per cavity) were administered into the pleural cavity of naïve mice and the number of infiltrating eosinophils assessed 48 h after injection. The results are expressed as mean±s.e.mean of six mice in each group. *$P<0.01$ when compared to PBS-injected animals.

Blockade of PAF receptors regulate the release of eotaxin and eosinophil recruitment in the allergic pleurisy

The possibility that endogenous production of PAF modulated eosinophil recruitment in the allergic pleurisy was investigated by using the PAF receptor antagonist UK-74,505. Pretreatment with UK-74,505 (1 mg kg^{-1}) significantly suppressed by 87% the recruitment of eosinophils observed 48 h after administration of antigen to sensitized mice (Figure 3A). As PAF induced significant local release of eotaxin, we examined whether blockade of PAF receptors would modulate eotaxin production in the allergic pleurisy. Our previous studies have demonstrated that eotaxin release peaks after 6 h in sensitized animals challenged with antigen (Klein *et al.*, 2001). Here, we demonstrate that pretreatment with UK-74,505 inhibited antigen-induced eotaxin production by 85% (Figure 4).

To confirm an important role of PAF receptors for the migration of eosinophils *in vivo*, PAFR$^{-/-}$ and wild-type mice were sensitized and challenged with antigen. As demonstrated in Figure 3B, eosinophil recruitment in PAFR$^{-/-}$ mice was inhibited by 50% as compared to wild-type mice. In PAFR$^{-/-}$ mice, the injection of PAF failed to induce a significant recruitment of eosinophils as compared to PBS-injected animals (wild-type: PBS, $0.2\pm0.1\times10^5$ eosinophils per cavity; PAF 10^{-9} moles per cavity, 2.7 ± 0.8; PAFR$^{-/-}$, PAF 10^{-9} moles per cavity, 0.4 ± 0.1, $P<0.05$, $n=4$).

Cooperation between PAF and eotaxin

Next, we investigated whether sub-threshold doses of PAF and eotaxin could cooperate to induce eosinophil recruitment *in vivo*. As seen in Figure 5, a sub-threshold dose of eotaxin (10 ng per cavity) and PAF (10^{-11} moles per cavity) failed to induce eosinophil recruitment in the pleural cavity of naïve mice when injected alone. Nevertheless, concomitant injection of PAF and eotaxin induced significant eosinophil recruitment that was greater than the somation of either mediator when injected alone (Figure 5). The injection of the mediators alone or in combination failed to affect significantly the levels of circulating eosinophils at 1, 4, 24 and 48 h after challenge, as compared to PBS-injected mice (data not shown).

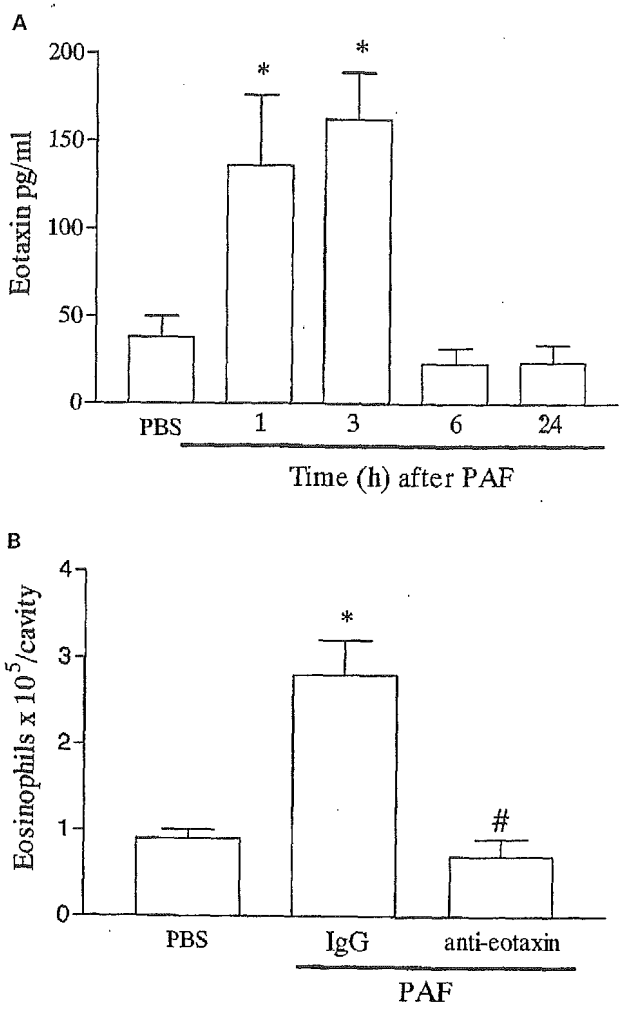

Figure 2 Time-course of the release of eotaxin into the pleural cavity after administration of PAF and effects of an anti-eotaxin polyclonal antibody on PAF-induced eosinophil recruitment. (A) Naïve mice were given an i.pl. injection of PAF (10^{-9} moles per cavity) and at different times after challenge (1–24 h), the pleural cavity of animals were washed, the cells centrifuged, and the supernatants used for the determination of eotaxin using a specific ELISA. (B) Naïve mice were pretreated with non-immune IgG (100 μg, i.p.) or purified anti-eotaxin polyclonal antibody (100 μg, i.p.) 30 min before the i.pl. injection of PAF (10^{-9} moles per cavity) and the number of infiltrating eosinophils assessed after 48 h. Results are expressed as mean±s.e.mean of six mice in each group. *$P<0.01$ when compared to PBS-injected mice and #$P<0.01$ when compared to animals treated with non-immune IgG.

Discussion

There are many experimental and clinical studies supporting a role for eosinophil recruitment and function in the pathophysiology of allergic diseases (Cara *et al.*, 1999). Thus, strategies which limit eosinophil migration and/or function *in vivo* may be relevant as novel therapy for the treatment of

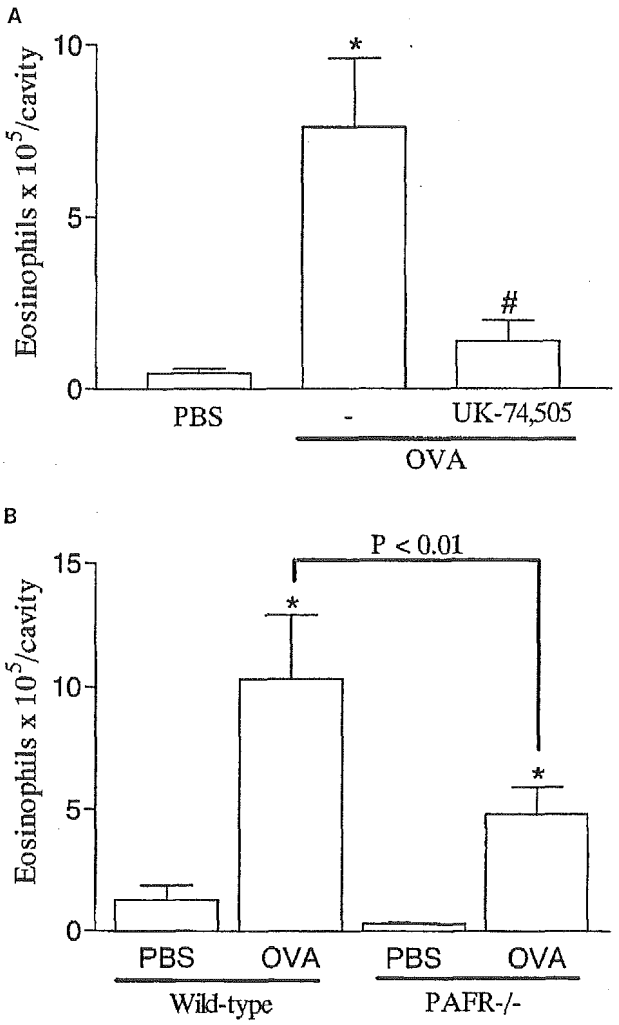

Figure 3 Effects of the PAF receptor antagonist, UK-74,505, and of PAF receptor deficiency on the eosinophil recruitment induced by allergen challenge in sensitized mice. (A) Mice were pretreated with UK-74,505 (1 mg kg^{-1}, i.p.) 60 min before the i.pl. injection of antigen (OVA, 1 μg per cavity) in sensitized mice and the number of infiltrating eosinophils assessed after 48 h. (B) Immunized wild-type or $PAFR^{-/-}$ received an i.pl. injection of antigen (OVA, 1 μg per cavity) and the number of infiltrating eosinophils assessed after 48 h. Results are expressed as means ± s.e.mean of six mice in each group. $*P<0.01$ when compared to PBS-injected mice and $\#P<0.01$ when compared to animals treated with drug vehicle.

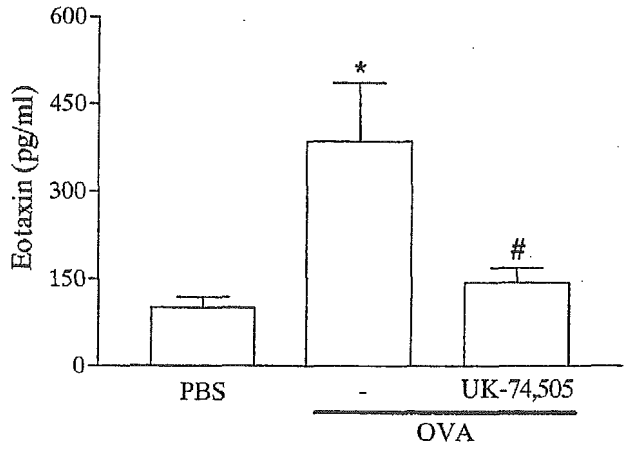

Figure 4 Effects of the PAF receptor antagonist, UK-74,505, on the release of eotaxin induced by allergen challenge in sensitized mice. Mice were pretreated with UK-74,505 (1 mg kg^{-1}, i.p.) 60 min before the i.pl. injection of antigen (OVA, 1 μg per cavity) in sensitized mice and the levels of eotaxin on the pleural wash assessed after 6 h. Results are expressed as means ± s.e.mean of six mice in each group. $*P<0.01$ when compared to PBS-injected mice and $\#P<0.01$ when compared to animals treated with drug vehicle.

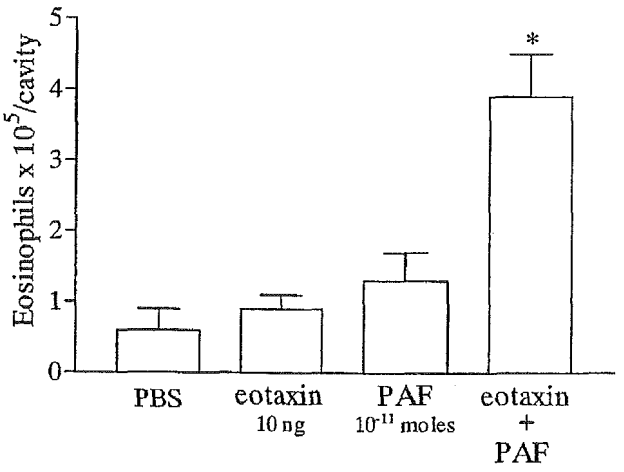

Figure 5 Cooperative effects of the injection of sub-threshold doses of eotaxin and PAF on eosinophil recruitment into the pleural cavity of mice. Mice were injected with phosphate-buffered saline (PBS, 100 μl), eotaxin (10 ng), PAF (10^{-11} moles) or with PAF and eotaxin and the number of infiltrating eosinophils assessed after 48 h. The results are expressed as means ± s.e.mean of six mice in each group. $*P<0.01$ when compared to mice injected with PBS or the mediators alone.

allergic diseases (Teixeira *et al.*, 1995; Giembycz & Lindsay, 1999). Chemokines are among the mediators which are thought to play an important role for the migration of eosinophils (and other leukocytes) *in vivo* (Murphy *et al.*, 2000). We have been particularly interested in understanding the mediators of the inflammatory process which regulate chemokine production and how chemokines interact with other mediators to induce the recruitment of eosinophils *in vivo*. We have previously demonstrated a role for the cooperation between SCF-driven LTB_4 release and eotaxin in mediating eosinophil recruitment *in vivo* (Klein *et al.*, 2000; 2001). Here, we investigated a role for PAF in driving eotaxin production and eosinophil recruitment in the allergic pleurisy model.

In agreement with *in vivo* studies in experimental animals and in humans (Henocq & Vargaftig, 1986; Silva *et al.*, 1991; Teixeira *et al.*, 1994; 1997a), injection of PAF induced a significant recruitment of eosinophils into the pleural cavity of mice. Interestingly, PAF-induced eosinophil recruitment was preceded by a rapid increase in the release of eotaxin into the pleural cavity. The kinetics of eotaxin release following PAF is slightly faster than that observed after antigen challenge in the allergic pleurisy and other models (Gonzalo *et al.*, 1996; Humbles *et al.*, 1997; Klein *et al.*, 2001). Moreover, PAF-induced eosinophil recruitment was suppressed by pretreatment with an anti-eotaxin antibody.